Using metal oxide gas sensors ~~for the~~ to estimate ~~of methane controlled releases: reconstruction of~~ the ~~methane mole fraction time-series and quantification of the release~~ emission rates and locations of methane leaks in an industrial site: assessment with controlled methane releases

Rodrigo Rivera Martinez[1], Pramod Kumar[1], Olivier Laurent[1], Gregoire Broquet[1], Christopher Caldow[3,4], Ford Cropley[1], Diego Santaren[1], Adil Shah[1], Cécile Mallet[2], Michel Ramonet[1], Leonard Rivier[1], Catherine Juery[5], Olivier Duclaux[5], Caroline Bouchet[6], Elisa Allegrini[6], Hervé Utard[6], and Philippe Ciais[1]

[1]Laboratoire des Sciences du Climat et de l'Environnement, LSCE/IPSL, CEA-CNRS-UVSQ, Université Paris-Saclay, 91191 Gif-sur-Yvette, France
[2]Université de Versailles Saint-Quentin, UMR8190 – CNRS/INSU, LATMOS-IPSL, Laboratoire Atmosphères Milieux, Observations Spatiales, Quartier des Garennes, 11 Boulevard d'Alembert, 78280 Guyancourt, France
[3]Clean Energy Regulator, Discovery House, 47 Bowes St, Phillip ACT 2606, Australia
[4]Environment, CSIRO, Aspendale, VIC, 3195, Australia
[5]TotalEnergies - OneTech, Laboratoire Qualite´ de l'Air – 69360 SOLAIZE FRANCE
[6]SUEZ - Smart & Environmental Solutions; Tour CB21, 16 place de l'Iris, 92040 La Défense France

Correspondence: Rodrigo Rivera (rodrigo.rivera@lsce.ipsl.fr)

Abstract. Fugitive methane (CH_4) ~~emission~~ emissions occur in the whole chain of oil and gas production, ~~from the~~ including from extraction, transportation, storage, and distribution. ~~The detection and quantification of such emissions are conducted usually from~~ Such emissions are usually detected and quantified by conducting surveys as close as possible to the source location. However, these surveys are ~~labor intensive, costly and they do~~ labour intensive, are costly, and fail to not provide continuous ~~monitoring of the emissions~~ emissions monitoring. The deployment of permanent ~~networks of sensors~~ sensor networks in the vicinity of industrial CH_4 emitting facilities would overcome the limitations of surveys by providing accurate ~~estimates~~ emission estimates, thanks to continuous sampling of ~~the plumes. High~~ emission plumes. Yet high precision instruments are too costly to deploy in such networks. Low-cost sensors ~~like Metal oxide semiconductors~~ using a metal oxide semiconductor (MOS) are presented as a cheap alternative for such deployments due to ~~its~~ their compact dimensions and to ~~its~~ their sensitivity to CH_4. In this study~~we test~~, we demonstrate the ability of two types of MOS sensors ~~from the manufacturer Figaro®~~ (TGS 2611-C00 and TGS 2611-E00) ~~deployed in six chambers to reconstruct an actual signalfrom a source in open air corresponding to a series of controlled CH_4 releases and we assess the accuracy of the emission estimates computed from reconstructed CH_4 mole fractions from voltages measurements of these sensors. A baseline correction of the voltage linked to background variations is presented~~ manufactured by Figaro® to reconstruct a CH_4 signal, as measured by a high-precision reference gas analyser, during a 7-day controlled release campaign conducted by TotalEnergies® in autumn 2019 near Pau, France. We

propose a baseline voltage correction linked to atmospheric CH_4 background variations per instrument based on an iterative comparison of ~~neighboring observations. Two~~ neighbouring observations, *i.e.* data points. Two CH_4 mole fraction reconstruction models were compared~~,~~ : multilayer perceptron (MLP) and ~~2nd degree polynomial, providing similar performances meeting our target requirement on all the chambers when the input variable is the TGS 2611-C00 sensor. The emission~~ 2nd degree polynomial. Emission estimates were then computed using an inversion approach based on the adjoint of a Gaussian dispersion model~~obtaining promising results with an~~ . Despite obtaining emission estimates comparable with those obtained using high precision instruments (average emission rate error of 25% and ~~a~~ average location error of 9.5 m~~.~~), the application of these emission estimates is limited to adequate environmental conditions. Emission estimates are also influenced by model errors in the inversion process.

1 Introduction

~~Fossil fuel anthropogenic~~ A recent study suggests that in the decade 2008-2017, methane (CH_4) emissions ~~related to~~ from the production, ~~exploitation and transport of~~ transportation, storage, and distribution of fossil fuels (e.g. coal, oil, and natural gas~~, account~~) accounted for 35% of global anthropogenic CH_4 emissions (Saunois et al., 2020). ~~Emissions from natural gas production occur along the chain from extraction, transportation, storage, distribution and use~~These emissions are typically quantified through emission inventories. Emissions estimates reported by inventories rely on information from activity data (*i.e.* human activities contributing to emissions like fuel consumption) and emission factors ~~. Emission factors are different between sites, technologies, operating modes and are not stationary~~(i.e coefficients that relate the activity data to emission rates). Although generalised emission factors can be used to develop emission inventories, emission factors can vary between different sites depending on site-specific technologies, and operating modes, which makes the upscaling of fugitive CH_4 emissions highly uncertain (Alvarez et al., 2018). For instance, estimated emissions from the oil and gas supply chain in the US in 2015 constrained from ground based and aircraft measurements were found to be 60% higher than the ~~EPA~~ Environmental Protection Agency (EPA) inventory (Alvarez et al., 2018). More generally, the characterization of CH_4 emissions from complex processes based on ~~static~~ generalised emission factors can be ~~challenged when the~~ underestimated when best practices are not followed by operators (Riddick et al., 2020).

Atmospheric measurements are increasingly used to detect and quantify CH_4 leaks from industrial facilities. ~~The measurements~~ These methods primarily involve measuring methane mole fraction downwind of the facility. Measurements are often interpreted with local-scale dispersion models using atmospheric inversion methods to infer the CH_4 source location and emission ~~rates~~rate, see e.g. (Kumar et al., 2022). Current approaches generally consist ~~in~~ of conducting atmospheric surveys of the enriched ~~concentration~~ mole fraction plume created by the emitting source. ~~Difficulties are the~~ There are several challenges with this approach: accessibility to sample ~~the plumesfrom emitting locations, labor~~ downwind emission plumes, labour requirements, and instrument costs, given that surveys ~~currently~~ may employ expensive high precision research-level CH_4 instruments ~~, such as Cavity~~ using techniques such as cavity ring-down ~~spectrometers~~ spectrometry (CRDS). Further, downwind surveys do not provide continuous ~~monitoring of the sources~~ source monitoring (Travis et al., 2020). The de-

ployment ~~and functioning of mini-networks~~ of networks of continuous monitoring ~~sensors for~~ CH_4 ~~mole fractions~~ sensors around emission sources is an alternative to surveys, but the costs of each instrument remain a limitation. Advances in the development of low-cost sensors facilitates the deployment of dense ~~sensors'~~ sensor networks to increase ~~the coverage of a site (Kumar et al., 2015; Mead et al., 2013). Permanent deployment of a network of sensors can overcome limitations in the quantification of leaks and help to better characterize the plumes by limiting the impact of~~ site coverage (Kumar et al., 2015; Mead et al., 20 . The use over long periods of time of dense networks of sensors deployed permanently increase the ability to identify the structures of the observed plumes, to improve the atmospheric transport modelling ~~uncertainties. In addition,~~ parametrization for the simulation of these plumes, and thus to improve the accuracy of the quantification of the ~~theoretical study of Chamberland and Veerav proved that performance is improved in differentiation of known signals from noise by increasing the sensor density in an area~~leaks based on this modelling.

In ~~later years, an increase in the~~ recent years, growing interest in low cost and low power sensors ~~to be used in dense networks~~ for use in relatively dense networks has led to the study of different kinds of sensors to measure pollutants and trace gases like carbon dioxide (CO_2) or CH_4. One of the most common low-cost sensors technologies for the detection and quantification of CH_4 emissions is metal oxide semiconductors (MOS). MOS sensors are composed of a metal oxide sensing material~~and a heaterensuring that the sensing material reaches temperatures between 300 to 500 °C~~, incorporating an integrated heater. A chemical reaction affects the electrical conductivity of the sensing material in the presence of an electron donor gas such as CH_4 (Özgür Örnek and Karlik, 2012). ~~The advantages of MOS sensors are that they are compact and very well suited to long time deployment due to their resilience to extreme weather conditions. However, their sensitivity is affected by environmental parameters (~~However, MOS sensor sensitivity is also affected by other environmental parameters such as temperature and relative humidity ~~) (Popoola et al., 2018)and VOCs~~(Popoola et al., 2018); they also present low accuracy and may drift with time (in the form of a decrease in the ~~conductance~~ conductivity of the sensing material), requiring periodic re-calibrations (Riddick et al., 2020; Shah et al., 2023, 2024), and the need ~~of~~ for a constant power supply due to the heater material (Shah et al., 2023).

The Taguchi Gas Sensors (TGS) ~~commercial MOS from the Figaro® manufacturer, were~~ is a commercially available range of MOS sensors manufactured by Figaro®, which have been widely tested in different environments (including under controlled conditions and ~~field deployment due to their sensitivity to~~ during field deployment) due to the CH_4 ~~(Eugster et al., 2020; Eugster and Kling, . The standard technique to derive a calibration methodology is to collocate these MOS sensors~~ -sensitivity of certain TGS models (Eugster et al., 2020; Eugster and Kling, 2012; Riddick et al., 2020; Collier-Oxandale et al., 2018; Bastviken et al., 2020; van den . A standard technique for calibrating these sensors has involved collocating them with a high precision instrument used as a reference, ~~then apply~~ and then applying empirical equations or data-driven approaches ~~(Eugster et al., 2020; Eugster and Kling, 2012; Casey e~~ to derive CH_4 mole fraction (Eugster et al., 2020; Eugster and Kling, 2012; Casey et al., 2019; Bastviken et al., 2020; Collier-Oxandale et . In a previous work (Rivera Martinez et al., 2021) we ~~have~~ studied the possibility of using ~~Artificial neural Networks~~ artificial neural networks (ANN) to reconstruct ~~the variations of~~ variations in CH_4 mole fractions in room air under controlled conditions from three types of Figaro sensors (TGS 2600, TGS 2611-C00, and TGS 2611-E00). A following study (Rivera Martinez et al., 2022) ~~analyzed~~ analysed the potential to reconstruct ~~spikes of~~ CH_4 spikes generated on top of ambient air observations, that

corresponded to typical signals from leaks at industrial sites, employing two types of Figaro sensors (TGS 2611-C00 and TGS 2611-E00). That study made a ~~thorough~~ comprehensive comparison of the performance of five models for the reconstruction of CH_4 mole fraction.

The next logical step is to test the ~~performances~~ performance of the same sensors to reconstruct CH_4 mole fraction from real leaks, and to use ~~the~~ reconstructed mole fractions to quantify and localise emission rates. ~~To our knowledge, only one study attempted to do so. Riddick et al. (2020) quantified emissions of~~ Riddick et al. (2020) quantified CH_4 emissions from a gas terminal using a Figaro TGS 2600~~included in a logger system controlled by an Arduino Uno. The logging system was located~~ , deployed 1.5 ~~m from a point~~ km from the emission source. To reconstruct CH_4 mole fractions from voltage observations, ~~Riddick et al. (2020)~~ the authors developed an empirical equation considering the measured voltage, temperature~~and the humidity . Then, a~~ , and relative humidity from a nearby meteorological station and then applied a Gaussian plume model ~~was used~~ to quantify the emission rate using ~~information from the~~ reconstructed CH_4 mole fractions and ~~wind information from a nearby meteorological station. Their estimates of the emissions rates had an average value~~ local wind information. Their estimated average emissions of 9.6 g CH_4 s^{-1}~~and reached a maximum~~ , with a maximum emission rate of 238 g CH_4 s^{-1}, given corresponding ~~to enhancements of the~~ CH_4 mole ~~fractions~~ fraction enhancements of between 2 ppm to 5.4 ppm within the plume. Their ~~estimates based on a Figaro sensor~~ Figaro-based emission estimates were not confronted with ~~high precision instruments~~ corresponding emission estimates derived using a high precision gas analyser nor with an independent knowledge of the emission rate. Elsewhere, Riddick et al. (2022) studied the capabilities to detect and estimate CH_4 emissions of four Figaro TGS 2611-E00 sensors in a fence-line monitoring setup. Sensors were deployed closer to the emission source (30 m) and tested over a 48 hour period. Reported results showed detection consistency for emissions above 167 g CH_4 h^{-1} with an enhancement threshold of 2 ppm. However, the number of sensors used to compute the emission estimates was not specified, particularly given the spatial distribution of the sensors and varying wind speed.

In this study, we test the ability of a network of several Figaro sensors to reconstruct ~~the~~ atmospheric CH_4 ~~atmospheric~~ mole fraction enhancements from a series of controlled releases of known ~~magnitudes and duration in open air~~ magnitude and duration to the open atmosphere at a facility called TADI (see Methods), and to infer the emission rate of each release by an inverse ~~modeling~~ modelling approach. The accuracy of ~~the~~ CH_4 mole fraction reconstruction is evaluated against collocated accurate CH_4 measurements from high precision CRDS instruments. The accuracy of the inverted emission locations and rates is evaluated against the known (controlled) location and magnitude using the inversion model of Kumar et al. (2022).

This study builds upon the research conducted by Rivera Martinez et al. (2022) and Kumar et al. (2022), demonstrating the potential for continuous monitoring of CH_4 emissions using cost-effective in situ sensors. Drawing from the insights derived from these two studies, it seeks to address the new challenges associated with the combination of both types of analysis~~.~~ , i.e reconstruction of CH_4 mole fractions from measured voltage variations and estimation of emission rates and location from CH_4 mole fractions. Firstly, the challenge arises in the deployment and management of ~~Figaro® sensorsonsite~~onsite Figaro sensors, an issue not present in Rivera Martinez et al. (2022), as well as extracting CH_4 ~~concentrations~~ mole fractions from measurements that are impacted by more complex perturbations. For instance, the background air in ~~Rivera Martinez et al. (2021, 2022)~~ Rivera Martinez et al. (2021, 2022) was less polluted than ~~the one~~ air from an industrial site such as TADI. Moreover, the en-

vironmental conditions, especially in terms of temperature and ~~moisture~~water mole fraction, in these previous studies were smooth and not representative of ~~the real~~ field conditions as encountered in this new study. Secondly, the prescriptive precision and accuracy targets for CH_4 reconstructions outlined in Rivera Martinez et al. (2022) were established as generic targets, fitting for a variety of data processing strategies intended to quantify emissions from industrial sites. The specific observation and modelling strategy implemented in Kumar et al. (2022) to localise and quantify point source emissions carries its own set of precision/accuracy requirements. In particular, this strategy strongly relies on the ~~characterization~~ characterisation of gradients across ~~the~~ measurement stations of ~~concentration~~ mole fraction averages over time or wind sectors, which makes the derivation of nominal requirements on the reconstruction of CH_4 spikes or the CH_4 time series quite complex. Furthermore, such requirements should be weighed against the modelling uncertainties associated with the corresponding Gaussian plume model inversions. Ideally, the uncertainties related ~~to the~~ with CH_4 mole fraction data would not significantly ~~add to~~ contribute towards the total uncertainty when ~~combining them~~ combined with uncertainties from the modelling framework. This, however, does not necessarily mean that they should be much smaller than the latter. The direct comparison of the results obtained in this study with CH_4 mole fraction data derived from ~~the~~ Figaro sensors and those from Kumar et al. (2022) provides insights into whether this objective is achieved.

Therefore, for 33 controlled releases at the TADI facility, we employed fixed-point measurements from both high precision CRDS instruments and low-cost ~~TGS~~TGSs. A considerable fraction of the TGS measurements were used for training models to reconstruct CH_4 ~~mixing ratios~~ mole fractions from measured TGS resistance and other variables. When reconstructing ~~the~~ CH_4 ~~concentrations~~mole fractions, we proposed a minimum accuracy target ~~for CH_4 reconstruction models at~~ of 15% ~~of~~ the amplitude of the largest observed ~~excess~~ mole fraction enhancement within a release. This corresponds to accuracies ~~going~~ from 0.3 ppm for a release causing a maximum ~~excess~~ enhancement of 2.4 ppm ~~,~~ up to 18 ppm for a maximum ~~excess~~ enhancement of 120 ppm. This accuracy is consistent with the accuracy requirement ~~set~~ imposed in our previous study where we used TGS sensors to reconstruct CH_4 spikes created in a laboratory experiment (Rivera Martinez et al., 2022). However, the relevance of this target is implicitly re-assessed through the use of the reconstructed time series in the inversion scheme from Kumar et al. (2022).

The plan of the study is as follows. Section 2 presents the TADI 2019 controlled releases campaign, the logger systems, the data treatment, the models employed to reconstruct CH_4 concentration from TGS data, and the atmospheric inversion approach. The ~~data treatment,~~ comparison of the models for the reconstruction of CH_4 and the inversion results for rates and locations of different releases are ~~analyzed~~ analysed in section 3. Results are discussed in Section 4, and ~~conclusion~~ conclusions are given in section 5.

2 Methods

2.1 ~~Sampling strategy at the~~ TADI-2019 campaign

In October 2019, TotalEnergies® ~~conducted an experiment with~~ performed multiple controlled releases at the TotalEnergies Anomaly Detection Initiative (TADI) facility, to investigate the capability of different detection and quantification ~~of different~~

~~technologies for local emissions produced on~~ techniques of CH_4 emissions from industrial facilities. The TADI test site is ~~designed and operated by TotalEnergies® to test different technologies and methodologies of detection and quantification of gas leaks in an industrial environment, such as oil and gas production facilities. The platform is~~ located northwest of Pau, France, with an approximate area of 200 m~~× 200 m. The site~~ ^{2}. It is equipped with ~~a series of~~ infrastructure typical of oil and gas facilities (pipes, valves, tanks, ~~, and other equipment commonly found on oil and gas facilities~~ etc) to simulate 'realistic' leaks. The terrain is flat but includes different obstacles that can affect the dispersion of the gases released to the atmosphere. ~~This~~ Our experiment consisted of 41 controlled releases of CH_4 and ~~CO_2~~ CO_2, covering a wide range of ~~emissions~~ emission rates of between 0.15 and 150 g CH_4 s^{-1} ~~and~~ , with durations ranging between 25 to 75 minutes. We participated ~~to~~ in this experiment to develop and test inverse modelling frameworks within the TRAcking Carbon Emissions (TRACE, https://trace.lsce.ipsl.fr/) program for the estimation of emission location and rates based on CH_4 mole fractions from high precision instruments (Kumar et al., 2022). We presented the inversion results for 26 releases from single point sources based on two inversion approaches, one relying on fixed-point measurements, and the other one on mobile near-surface measurements (the latter had already been documented in ~~(Kumar et al., 2021)~~Kumar et al. (2021)). In both cases, the ~~estimates of the emissions~~ emission estimates relied on CH_4 mole fractions from high precision instruments, and on a Gaussian plume model to simulate the local atmospheric dispersion of CH_4. The results from Kumar et al. (2022) ~~proved to be relatively good, with an error in the release rate estimates from fixed-point measurements between ~~~for point source emissions yielded an emission rate error of between 23 to ~ 30 % and ~~an error in the location of the point sources~~ a localisation error (within a 40 m × 50 m area) of between 8 and 10 m.

The controlled releases were emitted ~~at different heights up to~~ from heights of between 0.1 m and 6 m above ~~the ground~~ ground level, and inside the 40 m × 50 m ATEX (ATmospheres EXplosibles) zone of the TADI facility (see Fig. 1).

~~More information on the site infrastructure and on these experiments in~~

2.2 Controlled releases and sampling configuration

A total of 41 controlled releases were conducted over a seven day period, between 2 October 2019 ~~are presented respectively in Kumar et al. (2021) and Kumar et al. (2022).~~

~~The multiple controlled releases experiment was conducted from~~ and 10 October ~~2, 2019, to October 10,~~ 2019. Six releases corresponding to low wind speeds (< 0.6 m s^{-1}) were not used for the inversion as in Kumar et al. (2022), since measurements made in low winds are not suitable for atmospheric inverse modelling. They could however be used in the training of CH_4 mole fraction reconstruction models. The two largest releases produced high CH_4 mole fraction plumes that affected the amplitude measured by the TGS sensors, such that it was not possible to distinguish large CH_4 spikes from medium and small spikes from voltage drop measurements (see fig A3) and, hence, they were also removed. Therefore, our study is focused on 33 from the initial 41 controlled releases conducted during the campaign. Table A1 details the releases that were measured by each chamber. The protocol followed in the selection of releases used for the training and testing of reconstruction models is explained in section 2.6.

Our atmospheric sampling configuration for measuring CH_4 is shown in figure 2. It consisted of placing 16 sampling lines (of 6.35 diameter) on the ground~~connected on one end to air intakes in tripods at heights~~ , with one end of each line attached to

tripods of between 2.75 ~~to~~ and 3.50 m high around the ATEX zone~~and on~~ , serving as air inlets, and the other end of each line connected to a pump flushing at 6 LPM (KNF N811 with PTFE diaphragm). The lengths of the sampling lines varied from 10 m to 100 m~~connecting each tripod air intake to~~ , connecting each air inlet to the CH_4 ~~measurement instruments located~~ sensors inside a tent. The pump was connected upstream ~~from~~ of the high precision instruments (Picarro CRDS or LGR), a chamber containing a series of TGS CH_4 sensors, and other ~~sensors measuring environmental parameters such as~~ environmental sensors measuring relative humidity, pressure, and temperature. To maintain the inline pressure at atmospheric pressure, a vent was also connected to each sampling line (Fig. 2).

~~Table 1 summarizes~~ Table A5 summarises the species measured ~~,~~ and the identifiers of the reference high precision instruments. All reference instruments measured H_2O to provide dry ~~mole fractions of the species~~gas mole fractions. The analysers' sampling frequency ranges between 0.3 to 1 Hz. In a previous study by Yver-Kwok et al. (2015), it was proven that ~~those~~ these CRDS gas analysers ensure high precision measurements and a low drift over time, of less than one ppb per month~~. Yet, two calibrations were conducted before and after the campaign. On average 6-7~~ , although the datasheet specifies a drift of 3 ppb per month (Picarro Inc.: Santa Clara, CA, USA).

On average 6 sampling lines were active for each release, each active line being connected to a high precision instrument and a TGS chamber. The lines were activated depending on wind direction. The strategy behind the distribution of the tripods around the emitting area and for the inversion was to ~~acquire continuously several measurements~~ continuously acquire several measurement points within the plume generated by each release, in addition to one or a few measurements points outside the plume (to ~~characterize the background~~ characterise the background mole fraction level upon which plumes enhancements can be assessed) for each release, regardless of the wind conditions (Kumar et al., 2022).

~~Summary of the species measured by each reference instrument. **Serial number / Code** **Identifier** **Species measured** CFKADS2286 / Picarro 1 Picarro CRDS G2401 CH_4, CO_2, CO CFKADS2301 / Picarro 2 Picarro CRDS G2401 CH_4, CO_2, CO CFKADS2194 / Picarro 3 Picarro CRDS G2401 CH_4, CO_2, CO CFKADS2131 / Picarro 4 Picarro CRDS G2401 CH_4, CO_2, CO CFIDS2067 / Picarro 5 Picarro CRDS G2201-i Isotopic $^{13}CH_4$, $^{12}CH_4$, $^{13}CO_2$, $^{12}CO_2$ CFIDS2072 / Picarro 6 Picarro CRDS G2201-i Isotopic $^{13}CH_4$, $^{12}CH_4$, $^{13}CO_2$, $^{12}CO_2$ LGR MGGA Los Gatos Micro-portable Greenhouse gas analyzer CH_4, CO_2~

2.3 Low-cost CH_4 sensors logger system and meteorological data

~~Seven chambers were assembled for the campaign. Table 2 displays the sensors included~~ Seven chambers containing TGS sensors were used. Table A6 shows the TGS and environmental sensors in each chamber, as well as the type of chamber~~, and the reference instrument with which each chamber was collocated, among other information~~. Each chamber contained at least three TGS units with voltage measurements sensitive to CH_4 and two other sensors measuring relative humidity/temperature and pressure/temperature. All ~~these~~ sensors were inserted inside an acrylic/glass or steel/glass chamber with volumes of 100 ml and 120 ml, respectively. The ~~sensitivity of TGS was controlled~~ logger system design was previously documented on Rivera Martinez et al. (2021) and Rivera Martinez et al. (2022). The measurement sensitivity of the TGS signal was determined by a load resistor connected in series ~~to~~ with the sensor (Figaro®, 2013, 2005)~~, two values of resistor were~~

used, 5K; the load resistance was either 5 kΩ and 50Kor 50 kΩ (see table 2 for detailsA6). An AB Electronics PiPlus ADC board mounted on a Raspberry Pi 3B+ recorded the voltage on drop across the load resistor, providing observations every 2s2 s. This voltage data is used for the characterization and reconstruction of the CH_4 signal. Consistency was observed between the two TGS 2611-E00 sensors installed on in chamber E, and only one sensor of this type is used in this study.

Measurements of environmental parameters from the other chambers , besides chamber E , all chambers other than chamber E had data gaps or recorded poor data for extended periodsor bad recordings occurring at releasesand were not included, including during releases, and were therefore not used. This study focuses on reconstructing CH_4 using data from TGS 2611-C00 and TGS 2611-E00 from chambers A, C, D, E, F, and H. Data from TGS 2600 data were discarded since this sensor did not respond to most of the CH_4 peaks during the releases (see Figure A1).

Summary of the specifications of the chambers, the tripods to which each chamber was connected, the captured releases and the reference instrument collocated with each chamber. **Chamber Figaro TGS Load resistor Other sensors Chamber type Tripod # of measured Referencesensors releases instrument**

2600 DHT22 1, 4, 6 2611-C00 BMP280 8, 9, 10 2611-E00 11, 14, 15 2600 SHT75 2, 7, 9 2611-C00 BMP280 14, 15, 16 2611-E00 2600 SHT75 2, 3, 9 2611-C00 BMP280 10, 11, 12 2611-E00 13, 16 2600* DHT22 1, 3, 4 2611-C00* SHT75 5, 10, 11 2611-E00* BMP180 12, 13, 16 2600 SHT75 2, 3, 4 2611-C00 BMP280 10, 11, 12 2611-E00 13, 14, 15 2600 SHT75 4, 5, 6 2611-C00 BMP180 7, 12, 13 2611-E00 14, 15

2.4 TADI controlled releases and meteorological data

A total of 41 controlled releases were conducted during the seven days of experiment, with release durations varying between 25 to 75 minutes. Because low wind conditions ($Ur < 0.6$ m s^{-1}) are not suitable for the atmospheric inverse modelling, six releases corresponding to such low wind conditions have been excluded for the inversion modelling here such as in Kumar et al. (2022) . However, they are used in the training of the CH_4 reconstruction models. There was no TGS measurements during the five releases corresponding to the last day of the campaign. Two largest releases produced high CH_4 mole fraction plumes that affected the amplitude measured by the TGS sensors on which it was not possible to distinguish large spikes from medium and small ones on the measured voltage (see fig A3) and they are removed from the study. One release was aborted due to technical problems at the site and is as well removed from this work. This study is thus focused on 33 out of the 41 controlled releases. A summary of these releases is shown in Table A1, where an 'x' indicates invalid data measured by the chambers. This invalidity is due to some releases producing small peaks over the background signal (with enhancements of less than 4 ppm), which the TGS sensors were unable to detect.

The protocol followed in the selection of the releases used in the training and test set for the reconstruction models is explained in section ??. A A meteorological station was installed on the TADI platform by TotalEnergies® with a sonic , with a 3D sonic anemometer at 5 m height above the ground surface above ground level (see Fig. 1), providing 1-minute averages of wind speed (UrUr), wind direction (θ), and of the standard deviation of wind speed on the three axes (σ_u, σ_v, and σ_w)amongst other parameters. The data of turbulence and meteorological conditions are used in the dispersion model. Table 3 gather 1 gathers general information for each of the 33 controlled release releases during which we have valid TGS measurements:

the duration of the release, the ~~actual~~ controlled release rate, the average wind speed over the duration of the release~~and an indication showing if it was selected for the~~ , and their inclusion status for inverse modelling.

2.4 ~~Reconstruction~~ Pre-processing of ~~spikes in CH_4 mixing ratios caused by~~ data from the ~~releases~~~~The chambers full of~~ TGS ~~sensors captured different portions~~ sensors

As well as resampling original observations with a 2 s time step to a longer 5 s time step, we also corrected the time offset due to air travelling from the air intakes to the instruments and the time delay from synchronisation between high-precision gas analysers and TGS chambers (between 2 to 3 minutes). We removed invalid TGS chamber data due to logging system faults. Finally, a baseline voltage correction was applied to the data from each sensor considering the entire campaign. Figure 3 illustrates the impact of the baseline correction, showing an improved agreement between corrected TGS voltage drop measurements for chamber A (for example) after the pre-processing steps and corresponding measurements from the reference gas analyser for one release.

2.5 Reconstruction of spikes in CH_4 mole fractions caused by the releases

The TGS chambers captured different segments of the plume with variations at high frequencies due to the distribution of the tripods with ~~regards~~ regard to the variable wind direction and due to ~~the~~ atmospheric turbulence. The typical signal measured by the chambers ~~is~~ shows a series of ~~spikes~~voltage enhancements, ranging between ~1 and ~15 minutes, corresponding to the plume lying over a slowly varying background signal associated ~~to~~ with remote emissions. The targeted signal is that of the difference between the spikes and the background CH_4 mole fraction level (Kumar et al., 2022). As an example, Figure ~~4~~ 3 shows 1-minute averages of CH_4 mole fractions measured by the reference instruments and the voltage from the TGS 2611-C00 at six tripods during release #25 (~~Q_s~~ Q_s = 5 g s^{-1}) ~~. We can observe that CH_4 of~~ showing consistency between measurements from the reference instrument and ~~TGS voltage show good consistency at this temporal resolution. Chamber~~ corresponding voltage drop measurements from the TGS chambers. Chambers A, C, and D were in the trajectory of the plume or very close to it measuring peaks ~~up to~~ of up to ~30 ppm~~, chambers~~ . Chambers E and F only captured ~~one~~ a single peak of ~10 ppm, and chamber H, one large peak of ~30 ppm. The mean wind speed during this release was ~~of~~ 3.12 m s^{-1} ~~and the wind direction had little variations , ranging~~ with small wind direction variations of between 270° ~~to~~ and 272°.

TGS sensors are known to be sensitive to variations ~~of~~ in humidity (H_2O ~~and T~~mole fraction) and temperature (T), affecting mainly the reconstruction of CH_4 baseline (*i.e.* when sampling background air without CH_4 enhancements), and thus the ~~characterization~~ characterisation of peaks above this baseline (Rivera Martinez et al., 2021, 2022). Two approaches can be used to correct for the effect of variable H_2O mole fraction and T on the TGS ~~signals baseline~~ voltage baseline signal and separate the voltage spikes from the baseline data in the time series. The first ~~one is the use of information from~~ method consists of using H_2O ~~and~~ mole fraction (retrieved from relative humidity, pressure and temperature) and T to correct the TGS ~~baseline signals correspond to these drivers~~voltage baseline signals. The second ~~approach is to detect the~~ method involves the detection of voltage peaks associated ~~to~~ with CH_4 spikes and ~~derive~~ deriving a baseline with a linear interpolation on non-peak voltages. ~~For some chambers due to logging system faults, we lost H_2O~~ Due to logging issues in some chambers, we did not

Table 1. Summary of the information for the controlled releases with single CH_4 point sources during the TADI 2019 campaign. Rows in ~~gray shows the~~ grey highlight releases with low wind speed conditions.

Release number	Duration (~~hh:mm~~minutes)	Emission rate (Q_s ($g\ s^{-1}$))	Average wind speed (U_r ($m\ s^{-1}$))	Used in ~~the~~ atmospheric ~~inverse modelling~~inversions
1	~~00:~~58	CH_4: 10	2.76	No
2	~~00:~~32	CH_4: 1	3.31	Yes
3	~~00:~~33	CH_4: 0.5	3.56	No
4	~~00:~~33	CH_4: 5	3.91	No
5	~~00:~~35	CH_4: 3, CO_2: 85	0.65	Yes
6	~~00:~~39	CH_4: 0.5	0.45	No
7	~~00:~~46	CH_4: 5.0	0.80	No
8	~~00:~~50	CH_4: 0.5 & 0.75 & 0.5 *	1.41	No
9	~~00:~~38	CH_4: 1, C_2H_6: 0.5	1.46	Yes
10	~~00:~~38	CH_4: 0.5	2.17	Yes
11	~~00:~~30	CH_4: 0.16	2.39	No
12	~~00:~~46	CH_4: 1	0.93	Yes
13	~~00:~~44	CH_4: 0.2	0.26	No
14	~~00:~~55	CH_4: 0.5 & 1.0 *	0.07	No
15	~~01:01~~ 61	CH_4: 2	3.50	No
16	~~00:~~44	CH_4: 2	1.83	No
17	~~00:~~50	CH_4: 4	1.45	No
18	~~00:~~48	CH_4: 0.3	0.13	No
19	~~00:~~40	CH_4: 2.0	0.41	No
20	~~00:~~58	CH_4: 2 & 4 *	0.47	No
21	~~00:~~44	CH_4: 1	1.31	Yes
22	~~00:~~33	CH_4: 1, C_2H_6: 0.2	1.11	No
23	~~00:~~50	CH_4: 2	1.84	No
24	~~00:~~43	CH_4: 150	2.63	No
25	~~00:~~35	CH_4: 5	3.12	Yes
26	~~00:~~48	CH_4: 0.4	2.73	Yes
27	~~00:~~37	CH_4: 0.5	3.12	No
28	~~00:~~45	CH_4: 0.5 & 0.5 *	1.04	No
29	~~00:~~44	CH_4: 0.6	1.07	Yes
30	~~00:~~44	CH_4: 1	1.51	No
31	~~00:~~24	CH_4: 2	1.70	No
32	~~00:~~34	CH_4: 4	3.58	Yes
33	~~00:~~45	CH_4: 2	2.49	Yes

* Multiple source releases.

have complete relative humidity, pressure and T data ~~and the corresponding gaps in the H_2O and T time series prevent us from~~ which impeded us in defining a correction model. Therefore, in this study we ~~have~~ employed the second approach. ~~To justify our choice, we have trained a multilinear regression model to determine a baseline signal on TGS 2611-C00 from Chamber E corresponding to H_2O and T. The regression model was trained on using observations from midnight to 6:00 in the morning on the first day and we attempted to reconstruct baseline variations of TGS voltage from observations comprised between 18:00 to midnight on the same day. The results of the multilinear model are presented on Figure A2 (in addition to the derived baseline when using the second approach). The second approach which produce a better detection of the baseline signal is also shown (see Fig A2) where we do not need a training set or environmental variables because it consists in the detection of peaks based on an iterative process on fixed rolling windows and a comparison with neighbouring observations~~A comparison of both methods is shown in Figure A2 justifying our choice.

To reconstruct CH_4 mole fraction from TGS voltage measurements, we calibrated empirical models that derive relationships between TGS voltage and other input variables~~and true~~ , compared to CH_4 ~~observed~~ mole fraction measurements made by the high-precision ~~instruments~~gas analysers. The models are ~~calibrated (training) and evaluated (testing~~first calibrated (trained) and then evaluated (tested) using two independent subsets of ~~the data. Following the widespread practice in the training of data-driven models to standardize the input variables to prevent~~ data. To prevent a difference in the range of magnitudes from conditioning the determination of model parameters the input variables are standardised, we applied a robust transformation consisting in removing the median and dividing ~~the~~ input observations by their 1-99th quantile range. We selected the two reconstruction models that gave the best performances in our previous study (Rivera Martinez et al., 2022), namely a polynomial regression and a ~~Multilayer Perceptron~~ multilayer perceptron (MLP) model~~, described below.~~

~~Second-degree polynomials have proven to be robust to derive relationships between the TGS voltage signal related to spikes and the corresponding CH_4 concentration (Rivera Martinez et al., 2022). Its formulation is of the form:~~

$$\hat{y}_{CH_4}(x_1) = \beta_0 + \beta_1 x_1 + \beta_2 x_1^2$$

~~Where $\hat{y}_{CH_4}$ is the predicted CH_4 concentration, x_1 is the Corrected voltage of the TGS after removing the effects of the baseline.~~

~~Artificial neural networks have been widely used to derive non-linear relationships between predictors and independent variables in many applications, as a universal approximator method (Hornik et al., 1989) and for their generalization capabilities (Haykin, 1998). In previous studies (Casey et al., 2019; Rivera Martinez et al., 2021, 2022) ANN was employed to derive CH_4 concentrations from TGS observations on different sampling configurations (field and laboratory conditions) with good agreement between the reference observations and the outputs produced from the models.~~

~~The simplest architecture of an ANN is the multi-layer perceptron (MLP), conformed of a series of units (neurons) in fully connected layers. The inputs of any unit will be the weighted sum of the outputs of the previous layer, to which an activation function (ReLU, tanh, etc.) is applied. As a machine learning approach, it requires a training basis to learn the relationships, adjusting the weights of its connections, between the inputs and outputs using an iterative process known as~~

optimization. Problems of MLP models are either underfit of data, producing a high error on the train set which can be mitigated with a sufficiently large network, or overfitting, producing a high test error when they cannot generalize to new examples. Regularizations terms and early stopping techniques are helpful to prevent overfitting (Bishop, 1995; Goodfellow et al., 2016) .

Here, we have trained the MLP model using the Adam optimizer (Kingma and Ba, 2014; Géron, 2019) resulting in 50, 10 and 5 units per layer with ReLU as the activation function for the hidden units. A regularization factor of α=0.05 and early stopping was used to prevent overfitting.. Description of the models and hyperparameter values (*i.e.* tunable parameters that influence the learning process of the model but not inferred from the data) are presented in SM. Three configurations of the input variables were tested: i) only with the TGS 2611-C00, ii) only with the TGS 2611-E00, and iii) with both TGS sensors at the same timesampling simultaneously. The results are shown in section 3.2.

2.6 Metrics for evaluation of the reconstruction

3.1. To assess the performance of the reconstruction models to provide dry CH_4 concentration mole fractions enhancements (above the background) from voltage observations of the low-cost sensorswe use a normalized drop measurements corresponding to the TGS sensors, we used a normalised root mean square error (NRMSE) per release, including information from the spikes and the background occurring in the duration of the release, defined in equation 1, the RMSE being weighted by the inverse of the maximum peak present in the release, defined as follows:

$$NRMSE = \frac{\sqrt{\frac{\sum(y_i - \hat{y}_i)^2}{n}}}{h_{max}} \quad (1)$$

where y_i is the actual concentrations (are the CH_4 mole fraction measurements provided by the high precision instrument), $\hat{y}_i$ are the reconstructed CH_4 mole fractions, n is the predicted concentration, n the number of observations present in the releaseand h_{max} each release, and h_max is the amplitude of the maximum peak mole fraction peak enhancement present in the release after removing the background. The normalization allows to compare the This normalisation allows us to compare performances across the different releases.

As mentioned earlier in section 2.2, the target signal on in this study is of CH_4 enhancements above the atmospheric background. We obtain this signal by subtracting the raw signal of voltage signal during the release from an inferred baseline voltage computed using the pic peak detection algorithm and a linear interpolation.

We consider

We pose as an acceptable notional target error for the reconstruction models to be under the reconstruction models of under 15% of the amplitude of the maximum peak inside the release, spike during the release; this error corresponds to a NRMSE $\leq$ 0.15ppm.

2.6 Selection of the training and test subsets for the reconstruction of CH_4 mole fractions as input of the atmospheric inversion of emissions

Defining ~~the appropriate training~~ an appropriate training data set is important to allow reconstruction models to derive sufficient information to ~~generalize and obtain good~~ generalise (*i.e.* to extend its performance to data not present in the training set) and to obtain good mole fraction reconstruction performances in the ~~test set. As well, the test~~ testing data set. In addition, the testing data set should be chosen to allow ~~evaluating the performances of the models~~ for the evaluation of model performances under a wide variety of conditions. Regarding ~~the~~ inverse modelling, in order to provide a meaningful assessment of the estimation of emission rates and locations, inversion should be conducted using reconstructed CH_4 mole fractions ~~that are not from~~ from outside the training data set to avoid introducing bias in the evaluations of errors. Furthermore, depending on ~~magnitude of~~ the magnitude of emission release rates, ~~the~~ atmospheric turbulence, and ~~the~~ locations/distances of the downwind active tripods from the emission sources, each of the six chambers ~~did not measure~~ could not be used to detect CH_4 mole fractions ~~in all the releases,~~ during each release; therefore a separate training and test set needs to be defined for each chamber.

~~The~~ These previous considerations constrain the selection of the training and ~~test sets from the data of~~ testing data sets from each chamber. The ~~test~~ testing data set of the releases for use in inversions was defined based on two criteria: 1) ~~the releases which have the~~ releases which yield reconstructed CH_4 mole fractions ~~by~~ from at least three chambers simultaneously, and 2) ~~the~~ releases corresponding to the more favourable wind speed conditions ($\sim\!\!\sim Ur\sim\!\!\sim$ $U_r \geq 1.4$ m s^{-1}) for inversions. We determined seven releases that meet these considerations ~~: release~~ (#2, #9, #10, #25, #26, #32 and #~~33. Because this test set was not sufficiently large for all~~ 33). Because this testing data set was of insufficient size for all of the chambers, we decided to increase it by using data from four more releases with low wind speed conditions ($0.65 \leq \sim\!\!\sim Ur\sim\!\!\sim$ $U_r \leq 1.31$) (~~release~~ #5, #12, #21 and #29). This selection led to a ~~test~~ testing data set of 40% of the releases. All remaining data were used as a training ~~set (Table ??)~~data set. The reconstruction models ~~are~~ were trained and tested only once per chamber, following the distribution of the releases from ~~table ??~~Table 2.

2.7 Atmospheric inversion of the release locations and emission rates

~~Our derivation of the release location and~~ Derivation of release locations and emission rates relies on ~~the~~ an atmospheric inversion framework developed and tested by Kumar et al. (2022)~~on the measurements of the~~ , which is based on measurements from high precision instruments. ~~This framework uses adjoint of a~~ The details of the approach and implementation for this atmospheric inversion framework are given in this publication and they are just briefly summarised here. This framework processes averages of the timeseries of the observed CH_4 mole fraction enhancements above the background from the different stations: from either the high precision measurements or from the reconstruction of CH_4 mole fraction based on the TGS sensors that is detailed above. For each station, these averages correspond to temporal averages within 2 to 7 bins of the observations defined by sectors of wind directions that are of equal ranges during the release (see below the practical definition of the wind sectors). The atmospheric inversion relies on the simulation of these average CH_4 mole fractions using a Gaussian plume model. It uses the adjoint of this Gaussian plume model to simulate the sensitivity of ~~the~~ these average CH_4 mole

Table 2. Summary of the releases included in the training data set and ~~test~~ testing data set of the CH_4 reconstruction models. The ~~mixing ratios~~ mole fractions modelled for the test set are also used as input of the inversion model to infer the ~~emission rate of~~ CH_4 emission rate and their location.

Chamber	Releases in the training set	Releases in the test set	Number of releases in the training set	Number of releases in the test set	Percentage of ~~releses~~ releases in th training/test set
A	6, 7, 8, 11, 14, 15, 16, 17, 18, 19, 20, 24, 27, 28, 30	2, 5, 9, 10, 21, 25, 26, 29, 32	15	9	62.5 % / 37.5 %
C	14, 15, 17, 18, 19, 20, 22, 24, 27, 28, 30, 31	9, 10, 21, 25, 26, 29, 32, 33	12	8	60 % / 40 %
D	6, 7, 8, 13, 14	5, 9, 12, 25	5	4	55.5 % / 44.5 %
E	3, 4, 6, 7, 8, 13, 14, 19, 20, 22, 23	2, 5, 9, 12, 21, 25, 26, 32, 33	11	9	55.5 % / 44.5 %
F	3, 4, 6, 7, 8, 13, 14, 15, 18, 19, 20, 22, 24	2, 5, 9, 10, 12, 21, 25, 29	13	8	62 % / 38 %
H	1, 3, 4, 13, 14, 18, 19, 20, 23, 24, 28, 30	2, 21, 25, 26, 29, 32, 33	12	7	63 % / 37 %

fraction enhancements above the background at a measurement location to the emissions at all potential source locations. This computation implicitly informs about the numerical operator corresponding to the simulation with the Gaussian plume model of the average CH_4 mole fraction enhancements above the background per wind sector and station as a function of the source location and rate. For each release, based on these sensitivities, the optimal horizontal and vertical location and emission rate are derived ~~based on the minimization of~~ as the horizontal and vertical location and rate minimising the root sum square (RSS) misfits between averages of the observed and simulated CH_4 mole fraction enhancements above the background. ~~The bins of the measurements and of the simulated mole fractions for the averages correspond to sectors of wind directions of equal ranges during the release. The~~ In practice, optimal release location and ~~rates are searched~~ emission rates are identified simultaneously, looping on a finite but large ensemble of potential locations, using an analytical formulation of the problem to derive the optimal rate and corresponding RSS misfits for each potential location and then identifying the optimal location and rate providing the smallest RSS misfits. The 40 m × 50 m (horizontally) × 8 m (vertically) volume above the ATEX zone is discretized with a

high resolution (1 m × 1 m horizontally and 0.5 m vertically) 3D grid to define ~~the~~ a finite ensemble of potential locations. The inversion exploits the change of wind direction during a release at the different measurement locations and the corresponding variations and spatial gradients in average mole fractions ~~respectively at and~~ between the different measurement locations ~~crossed~~ intersected by the plumes to triangulate the release location. The amplitude of ~~the~~ mole fraction enhancements directly constrains the release rate estimate.

The Gaussian model ~~and its adjointare~~ (in practice: its adjoint) is driven by averaged wind directions and averaged turbulence parameters derived from 3D sonic anemometer measurements, using the same bins for these averages as for ~~the~~ mole fractions. Those bins are ~~defined~~ derived during each release based on the analysis of 1-min averaged wind directions~~. These bins partition the lower and~~ : they correspond to a partition of the lower to upper range of potential 1-min average wind directions, ~~and they have~~ into wind sectors of equal width in terms of range of wind directions. The total number of bins during this initial partition is defined as the rounding integer of the division of the release duration (in min) by approximately 7 min. However, only bins gathering at least four 1-min averages are retained. The aim is that the mole fraction and meteorological averages are representative of a timescale that is long enough for use in or comparison to the Gaussian model. ~~Depending~~ This explains why, depending on the releases, the number of bins ranges between 2 and 7.

~~Here~~In this work, we slightly revise the reference computations of release location and rate estimates based on ~~the~~ mole fractions from high precision instruments from Kumar et al. (2022). Indeed, in order to compare the release location and rate estimates from such a reference and ~~the one derived here~~ to the results based on the TGS sensors, we restrain the set of high precision observations that are used in the reference computation to the station and time corresponding to ~~the~~ data availability from the TGS sensors.

3 Results

3.1 ~~Pre-processing of the data from the low-cost CH_4 sensors~~

~~Original observations with a time step of 2 s were resampled to 5 s. We corrected the time offset corresponding to delays of the air travel through the air intake from the tripods to the instruments, time delay from synchronization between analysers and chambers. Also, we removed invalid data produced by the logging system on each chamber. The baseline correction was then applied for each sensor chamber considering the entire campaign. As an illustration of the impact of the baseline correction Figure 3 shows the signal corresponding to one release for the chamber A after these pre-processing steps. The corrected signal in the TGS voltage measurements showed better agreement with the reference between the occurrences of spikes and phases.~~

3.1 Reconstruction of CH_4 mole fractions

Due to the diversity of the emission rates across the controlled releases, environmental conditions, ~~distribution of the tripods and~~ the spatial distribution of air inlets and the selection of the training and ~~test~~ testing data sets for each chamber, there is no single release that can be viewed as representative for the test set across the chambers. Yet, we chose release #25 as an example

of the signal measured across ~~the chambers and the reconstructed signal for each chamber~~ all the chambers. The reconstructed signal using the MLP model ~~(Figure 5) and the 2nd~~ is shown on Figure 5 and for the 2nd order polynomial model ~~(Figure 6), for~~ on Figure 6 respectively. For each chamber we shown the reconstructed CH_4 mole fractions estimated using only the type C sensors (red), the type E sensor (yellow) and both sensors used as inputs for the models at the same time (green).

We found that both the MLP and ~~2nd degree polynomials gave~~ 2nd degree polynomial models had similar performances across the releases, regardless of the chamber used for ~~the~~ CH_4 mole fraction reconstruction. For two releases ~~on~~ sampled by chamber A (release #10 and #26, see Fig A6 and A9 for MLP model and A11 and A12 for the polynomial model respectively)~~where amplitudes are~~ , characterised by amplitudes below 10 ppm, the polynomial model provides a noisy signal as output regardless of the configuration of the inputs used. There were however some cases ~~on~~ in which the polynomial model ~~produced better outputs than~~ outperformed the MLP, for example, the four releases ~~on~~ sampled by chamber D where the MLP model produced a systematic underestimation of the reconstructed CH_4 mole fraction on the three configurations of inputs.

Regarding the ~~TGS types~~two TGS types tested in this work, the type C sensor ~~gave~~ used alone produced better reconstructions than both the type E ~~or~~ sensor alone, as well as both types used as ~~the same time as inputs for the model . The reconstruction of CH_4 with the type E sensor shows~~ simultaneous model input. Type E sensors showed phasing errors in the form of a slow decay after large spikes ~~. In addition, there are some cases where type E sensors showed a response whereas no spikes were measured~~ and uncorrelated spikes not detected by the reference ~~instrument. For example ,~~ gas analysers for example during release #9 from chamber D (Figure A5 and A10, for the MLP and the polynomial model respectively) ~~of chamber D shows few spikes between 10 to 30 ppm reconstructed from data of the type E sensor with the polynomial model which are not present on the reconstructed data from the type C sensor. Using~~ . Simultaneous use of both sensors (Type C and E~~sensors at the same time as training data for models~~) as model input produced outputs closer to ~~models trained only with~~ model outputs trained with only type C sensor ~~. Some cases of reconstruction with MLP model produced~~ data. MLP models also presented, for some releases, a saturation of the outputs (release #9, #12 and #25 for chamber D (Figure A5, A7 and 5), release #21 for chamber H (Figure A8)) or a systematic bias (releases #2, #10 and #26, see Figure A4, A6 and A9). For releases with ~~peaks'~~ peak amplitudes above 40 ppm, a systematic underestimation is observed regardless ~~the~~ of the reconstruction model or the sensor ~~'s type~~type, used as input.

~~On figure 7 , we present a summary of~~ Figure 7 summarises the performance of the reconstruction ~~of the signal on the test set , given~~ on the testing data set using the NRMSE error defined in eq. ~~1~~(1). All chambers ~~have~~ reached our target error ~~of~~ (NRMSE $\leq$ 0.15~~ppm, except for Chamber A with the polynomial model using as input the~~), except in three cases corresponding to models using type E sensor as input (chamber A for polynomial model and MLP and ~~the MLP model for chambers A and C as well for the type E sensor. With~~ chamber C for MLP). Imposing a stricter target requirement of NRMSE $\leq$ 0.1~~ppm~~, only Chamber H ~~met~~ satisfied the target error regardless of the ~~model or~~ reconstruction model or the sensor used. Performances are similar when using the type C sensor as ~~input regardless the model~~ model input regardless of the choice of model, across all the chambers. When ~~used both~~ using both sensor types at the same time as model input, the ~~2nd degree polynomial provide~~ 2nd degree polynomial provides better reconstruction than the MLP ~~specially on~~ model, especially for chambers C, D and H (NRMSE = 0.09, 0.09 and 0.04 ~~ppm~~ for the polynomial model and 0.11, 0.13 and 0.07 ~~ppm~~ for the MLP). Chamber D, ~~where~~

~~there is little training dataavailable~~characterised by having limited training data, produced a systematic lower error ~~with~~ when using the polynomial model than ~~with the MLP regardless~~ when using the MLP model, regardless of the input variable used.

In summary, the model used in the reconstruction is important only for ~~the cases where little information is available for the training. This was the case for chamber D where the polynomial model provides better performances than the MLP model. We also found~~ cases where there is limited information available for model training. We also conclude that Type C sensors alone produced a better reconstruction of CH_4 spikes than ~~Type E ones, and a combination of data from~~ either using Type E sensors alone or using both types of sensors ~~did not improve the reconstruction producing similar outputs than the other types~~as model input.

3.2 Release rate and location estimates based on the observations from the TGS sensors

~~Averages of mole fractions~~ Average CH_4 mole fraction enhancements above the background and of their spatial gradients are displayed for release #25 in figure 8. ~~The~~ This figure compares the values of reconstructions from the low-cost sensors ~~(with~~ using the MLP model ~~; see figure A14~~ (see figure **??** for the values corresponding to the polynomial model), with corresponding measurements made by the high precision ~~measurements, and of the~~ gas analyser. It also shows simulations resulting from ~~the~~ inversions assimilating either the reference high precision data or ~~the reconstructions from the low-cost sensors~~reconstructed TGS data. Since the best reconstruction performances were obtained when using the type C sensor, the inversion results presented here are based on ~~the reconstructions from those sensors only . For the~~ reconstructions from only this type of sensors. For release #25, used as an example here, the procedure to define average values per wind sectors ~~has~~ resulted in four bins~~of wind sectors~~ , with an approximate size of 10°. ~~Average mole fractions are derived from the six chambers.~~ To simplify the numbering when mentioning the reference instrument or the TGS, we refer to the chamber identifier X (REF-X and TGS-X respectively, with X the name of the chamber). The contour plot of the cost function is presented in figure **??** showing the controlled release location and the inversion estimated location when assimilating TGS data.

In general, the observed spatial CH_4 mole fraction gradients between the different stations ~~are~~ to be similar when considering the reference gas analyser measurements and the ~~estimates of~~ reconstructed CH_4 mole fractions from the TGS, except for few cases where the reference is ~~more consistent to the expected signal. For~~ better, for example for release #25 (see Fig. 8)~~observed gradient~~ . During release #25, observed gradients from TGS-D data underestimate the actual gradients given by REF-D for θ= 308.3° and overestimate them for θ = 279.2°, where θ is the average direction of the wind sector.

The modelled average mole ~~fractions~~ fraction enhancements and thus the modelled gradients assimilating reference data are very close, in general, to the ones from these reference data, although some discrepancies can occur, e.g., for release #25, for REF-H with θ = 279.2°, REF-C with θ =301.4° and θ =289.1° and REF-A with θ =301.4° and 308.3°. For most of the cases, the modelled gradients assimilating the TGS data are closer to ~~the modelled gradients~~ those assimilating the reference data than to the observed TGS ~~ones~~data. In addition, the observed TGS data, for some cases, is closer to the observed reference one than to the modelled gradients assimilating either reference or TGS data, highlighting the higher impact of the model error on the inversion than the reconstruction error of CH_4 mole fractions.

Figure 9 shows ~~the comparison of the~~ a comparison of emission rate estimates with corresponding ~~errors, and of the location errors for the different inversions~~ relative error in the estimation of emission rate and location error across the eleven releases ~~. In this figure ,~~ of the testing data set. This figure shows estimates assimilating CH_4 mole fractions from the TGS using ~~the reconstruction with the MLP models~~ reconstructions from the MLP model (see Figure A14 for ~~the~~ results when assimilating ~~the reconstruction~~ reconstructed mole fraction measurements based on the ~~2nd~~ 2nd degree polynomial model).

Regarding the release rate estimates, those from inversions assimilating the reference mole fractions bear an average error of 30% and those from the inversion assimilating data from the TGS sensors bear an average error of 25%.

In the case of the estimation of the release location, the assimilation of the reference data produces a slightly smaller average ~~error location~~ localisation error of 7.86 m (σ = 5.47 m) compared to 9.49 m (σ = 4.58 m) from the assimilation of TGS data. For five releases (#2, #10, #12, #25 and #26), the assimilation of reference data yields a better estimate of the location, and for one release (#21), both inversions yield similar ~~location~~ localisation errors.

In general, ~~estimates of the emission rate~~ emission rate estimates (see fig 9a) ~~from reference data and~~ derived using CH_4 mole fraction from reference gas analyser and reconstructed from TGS data are similar. For three releases (#12, #25 and #32), we observe large errors in the ~~estimate of the release rate~~ release rate estimate. Inversion assimilating reconstructed TGS data or reference ~~data~~ gas analyser mole fraction measurements highly underestimate the rate for release #5 (1.41 and 1.34 g CH_4 s^{-1} respectively, with ~~an actual emission~~ a controlled release rate of 3.0 g CH_4 s^{-1}) and strongly overestimate the rate for release #32 (5.14 and 6.55 g CH_4 s^{-1} respectively, with ~~an actual~~ a controlled release emission rate of 4.0 g CH_4 s^{-1}). ~~Reference data~~ Modelling using measurements from the reference gas analyser provide a slightly better estimation of ~~the location of releases than the TGS~~release locations than the using reconstructed TGS data. Only for releases #29 and #33, the inversion assimilating ~~TGS observations provide a slightly better location of the source~~ reconstructed TGS data provide slightly better source localisation. Conversely, for releases #2, #12, #25 and #26, the location error from the inversion assimilating ~~TGS observations~~ reconstructed TGS data is almost double ~~than the one of the reference~~ that derived using reference gas analyser measurements. The errors on the emission rate estimate from both inversions was smaller than 30% for most of the releases, except ~~on~~ for four cases, where errors reached 80% for the inversion assimilating reconstructed TGS data and 65% for the inversion assimilating reference ~~data~~gas analyser measurements, respectively. There were two cases, ~~the release~~ releases #26 and #33, when the inversion assimilating ~~TGS observations~~ reconstructed TGS measurements produced a much lower error (2.5% and 5.3% respectively) in the ~~quantification of the emission rate~~ emission flux quantification than the inversion assimilating reference gas analyser observations (20.9% and 22.7% respectively). The fact that the assimilation of the TGS reconstructed CH_4 data can yield better results than when using accurate CH_4 mole ~~fractions measured~~ fraction measurements made by the reference instrument highlights the impact of the transport model error (associated to the simulation of the average mole fractions with the Gaussian model) in the inversion process. These errors dominate the resulting errors in the estimates of the release rate and location when assimilating the reference data ~~Kumar et al. (2022)~~(Kumar et al., 2022). They appear to have a weight larger than that of ~~the errors in the~~ errors in reconstructed mole fraction from TGS data when assimilating these data.

Table 3. Comparison of the emission rate ~~estimates~~ estimate (Qe), location error (El) and relative error ~~on the~~ of flux rate estimates for ~~the~~ inversions assimilating ~~the~~ reference ~~data~~ gas analyser measurements and ~~the reconstruction of the CH_4 from the~~ reconstructed TGS ~~low-cost sensor based on~~ mole fractions using the MLP model.

Release N°	~~Actual emission~~N° Chambers	Controlled release emission rate ($g\ CH_4\ s^{-1}$)	Reference Q_e ($g\ CH_4\ s^{-1}$)	Reference E_l (m)	Reference error (%)	TGS Q_e ($g\ CH_4\ s^{-1}$)	TGS E_l (m)	TGS error
2	4	1.0	1.10	5.26	10.8	0.89	12.40	
5	4	3.0	1.34	21.57	55.2	1.41	19.55	
9	5	1.0	0.88	14.29	11.9	1.11	12.78	
10	3	0.5	0.40	9.29	18.9	0.42	10.80	
12	3	1.0	0.34	3.08	65.7	1.84	7.15	
21	5	1.0	0.63	3.61	36.1	0.66	3.61	
25	6	5.0	4.61	4.57	7.8	5.41	10.02	
26	4	0.4	0.31	5.10	20.9	0.39	10.10	
29	4	0.6	0.45	3.40	24.5	0.43	2.34	
32	4	4.0	6.55	10.55	63.8	5.14	10.28	
33	3	2.0	2.45	5.77	22.7	2.10	5.37	
Average error				7.86	30.7		9.49	
σ_{error}				5.47	20.3		4.58	

4 Discussion

~~Our study showed the capability of the signal from metal oxide sensors to produce estimates of the emission rate and location from controlled CH_4 releases typical of those expected from leaks in industrial facilities. The used baseline correction algorithm allows to extract the variations of voltages from the TGS signal related to the high frequency variation of the plume across the different sensors' inlets. We compared the performances of two models, 2nd degree polynomials and MLP, to reconstruct CH_4 mole fractions during the controlled releases for three configurations of inputs. The reconstructed CH_4 mole fractions were used as input to an inversion modelling framework to estimate the emission rate and location for each release. Results of inversions assimilating TGS data were compared with those assimilating reference (CRDS) data.~~

~~The correction of baseline in TGS sensors~~ Baseline voltage correction of TGS sensors, in this study, assumes that the targeted voltage signal measured by the sensors corresponds to a series of ~~spikes at high frequency produced by the plume reaching and leaving the inlet tube of the sensors~~high frequency spikes produced as a result of the emission plume intermittently intersecting the various sensor air inlets, due to ~~the~~ atmospheric turbulence and high frequency ~~variations of the wind~~ wind variations. Our approach of deriving a baseline ~~signal from observations surrounding the spikes in an iterative process,~~ voltage signal offers a suitable alternative to otherwise correct the TGS observations when little or insufficient information is available to derive ~~a~~

baseline an analytical baseline voltage correction model (e.g. from observations of H_2O measurements of H2O mole fraction and temperature). This approach is interesting for conditions when the environmental parameters are highly variable or models does baseline voltage correction models do not dispose of sufficient observations to derive robust relationships to correct for the effects of environmental variables on the sensors' baseline TGS baseline voltage signal. This case corresponds well with the measurements presented in this study. However, in some cases, the plume can touch the inlet tube of the sensors during a prolonged period producing a intersect the sensor air inlet for a prolonged duration resulting in a voltage signal not only having exhibiting high frequency spikes but also continuous varying resulting in continuously varying voltage enhancements above the backgroundbaseline voltage level. For those cases, this our baseline voltage method would not be able to distinguish the enhancements on sensors' voltage sensor voltage enhancements corresponding to the CH_4 plume from the background and then we mole fraction enhancements due to the plume as opposed to the atmospheric background; we would then need to reconsider the derivation of a option of deriving a voltage baseline based on environmental parameters (H_2O H2O mole fraction and T).

Regarding the type of sensor used in the reconstruction of TGS used in CH_4 mole fractionsfraction reconstruction, we obtain best performances using only with Type C sensor as input for the models(compared to the reference gas analyser) using only Type C sensors as model input. The fast decay observed on the for reconstructed CH_4 after the spikes mole fraction measurements after each voltage spike was attributed to the response time of the TGS sensor. The slow decay observed on Type E sensors was probably due to a combination of the response time and the carbon filter added on top of the sensitive material to improve the selectivityof gasesfilter integrated inside the sensor causing to improve CH_4 selectivity. Concerning the reconstruction models, the polynomial and the MLP models in general produced equivalent produced similar results with few differences. It This confirms our previous study (Rivera Martinez et al., 2022) in which where we observed that the performances of models to reconstruct CH_4 mole fractions fraction reconstruction models were mainly driven by the type of sensor used used sensor, rather than from the model chosen for the reconstruction . With a low content of information (only few the choice of reconstruction model. In cases with a low information content of (*i.e.* only few observed voltage spikes, limited range voltage range, and variability of the spike magnitude, frequency, and duration) in the training data set (e.g. when reconstructing the CH_4 mole fractions of fraction for chamber D), the 2nd degree polynomial 2^{nd} degree polynomial model provides more accurate mole fraction estimates than the MLP model. This is probably due to the distribution of the data in the training set that MLP used data distribution within the training data set used by the MLP model to compute its parameters, which does not represent not representing the same range of variations than the one in the test within the testing data set. For spikes with enhancements mole fraction enhancements of under 5 ppm, the MLP model with the Type C sensor signal as input , produced a more accurate reconstruction than either using the Type E or both sensor's types when used as inputs at the same time. The noise present sensor alone or using both sensor types simultaneously as model inputs. The combination of both sensors as input produced a reconstruction of CH_4 mole fractions similar to using only one of the sensors (TGS 2611-C00). This can be explained by the fact that both of the TGS signals are highly correlated and do not add more information to the model, and the phase mismatch between both input signals produced by the filter on TGS 2611-E00 sensor. The noise in the voltage signal on during some releases, for example release #26 on chamber A, were was not correctly removed in the

reconstruction with the Polynomial model . However during the Polynomial model mole fraction reconstruction. However, for the type C sensor, the MLP model reduces the noise on the signal producing voltage signal noise, resulting in a more accurate mole fraction reconstruction.

Regarding the inversion of emission rates and locations using the Gaussian gaussian plume model framework developed by Kumar et al. (2022), we obtained good estimates and performances with the reconstructed time series of CH_4 mole fraction spikes from voltage measurements of TGS sensors and the results are comparable to those obtained when assimilating the reference datacorresponding mole fraction measurements from the reference gas analyser. We observed that the simulated gradients of the Gaussian model assimilating observation gaussian model assimilating observations from the TGS chambers were close to the simulated gradients of the reference inversions (assimilating high precision measurementsmeasurements from the high precision gas analyser), even if the observed gradients were sometimes in a different direction. In most cases errors from both inversions ranges ranged between 2.5% and 55% except for release #12 and #32where , where the error reached 65% and 63% for simulated gradients assimilating the reference datarespectively , respectively, and release #12 with an error of 85% error for simulated gradients assimilating the TGS data. The overall inversion performance assimilating TGS data and reference data are good and consistent. The slightly better average performance in the release rate estimates using TGS data (25% error) than the estimates using reference data (30% error) is not significant in regards of the with regards to the overall variability of the results . It and highlights the weight of the model errors associated to with the simulation of the average mole fraction with a Gaussian model. The These results demonstrate that the errors in the release rate and location estimations from inversions using both reference and TGS data are dominated by these model errors model errors in the inversion framework. The errors in the reconstruction of the CH_4 mole fraction spikes from the TGS voltage data are thus sufficiently low for use in the inverse modelling problem analysed here.

One should note that, as mentioned on section 2.32.7, in this study, the reference inversions rely on a restrained subset of the reference data that match the available data from TGS sensors. Results from Kumar et al. (2022) , considering the entire dataset available on the reference instruments, yielded significantly improved results. considering the full reference dataset yielded significantly superior results.

Detection threshold and differentiation of emission types

Our methodology requires for emissions to be sustained for long enough to be captured within each sampling interval. The principal limitation of our method is the requirement for at least four 1-minute averages, restraining the detection of short-lived emissions. Another challenge lies in the detection of emission types, such as vented, combustion, or fugitive emissions. This aspect, out of the scope of our study, would require a detailed study of the characteristics of each kind of emission requiring additional tools to distinguish their individual particularities.

Limitations of the inversion framework

The inversion approach applied here, described for a single emission source only as required by the controlled releases experiments, can be easily extended to estimate emissions from multiple sources (see Singh et al. (2013)). However, estimating emissions from multiple sources may require a more denser network of sensors to constrain a larger number of parameters for all sources. However, significant uncertainties may arise in emission estimates when measurements are taken in very close

proximity to the emission sources. Our methodology requires that emissions be sustained long enough to be captured within the sampling intervals. The principal limitation is the requirement for at least four 1-minute averages, restraining the detection of short-lived emissions. Another challenge lies in the detection of emission types, such as vented, combustion or fugitive emissions. This aspect, out of the scope of our study, would require a detailed study of the characteristics of each kind of emission requiring additional tools to distinguish the particularities of them.

Density of sensor network

In our campaign, we deployed 7 chambers connected to air inlets placed on tripods at distances of between 40 and 50 m from the emission source to capture methane plumes under various conditions. Table 3 details the number of sensors used for emission flux estimations across the controlled releases. The optimal number of sensors for emission flux localisation and estimation is complex, influenced by varying emission rates, environmental conditions, and setup configurations. Notably, when examining cases with uniform emission rates (1 g CH_4 s^{-1}), such as releases #12, #2, and #21 (with 3, 4 and 5 chambers respectively), a configuration of 4 to 5 sensors consistently produced the lowest errors for both sensor types. Yet, release #21 demonstrated that even five sensors may not guarantee low errors if the plume capture is suboptimal due to environmental factors or sensor placement.

We can contrast our setup with Riddick et al. (2022), who used four sensors approximately 30 m away from the source, but without detailing their individual contributions to emission calculations. The optimal configuration of such a relatively dense network necessitates a thorough investigation, possibly through simulations of typical emissions and the strategic addition or removal of sensors to assess their impact. However, a comprehensive analysis of optimal network configuration was beyond the scope of our study due to the limited number of data points recorded.

Computational efficiency of the inversion framework

Our inversion framework, developed in Python 3.8 utilising numpy, pandas, and scipy libraries, efficiently computes the RSS matrix through vectorized operations and a nested for-loop. This approach achieves an average computation time per release of 0.1 seconds for the RSS matrix and 1.46 seconds for full code execution, including data preprocessing on an 8-core Apple Silicon M1 processor. The framework, which can be further optimised with multiprocessing, is detailed in Table A7, showcasing computational times across different releases. It effectively estimates emission rates and source locations on a fine grid (40m x 50m x 8m, discretized at 1m x 1m x 0.5m), demonstrating practicality for real-world applications at minimal computational costs.

While our work presents promising results regarding the use of low-cost MOS sensors for estimating CH_4 emission rates and locations, it ~~'s~~ is imperative to acknowledge the high degree of uncertainty associated with continuous emission monitoring (CM) solutions, as evidenced by the study conducted by Bell et al. (2023). In their study, various CM technologies were tested against a series of controlled releases, revealing a broad range of true positive rates, false positive rates, and significant errors in the estimation of emission rates. Bell et al. found considerable variability in the performance of CM technologies, with mean relative errors (MRE) ranging from -44% to +586% for release rates of between 0.1 ~~–~~ and 1 kg ~~/h and for release rates above 1 kg/h, an MRE~~ h^{-1}, and MREs ranging between -40% and +93% for release rates above 1 kg h^{-1}. These findings

underscore the current limitations and inconsistent performance of CM solutions, even under less complex conditions than typically encountered in the field. While our study is encouraging, it represents just one step in the progression of this approach. ~~Further research, rigorous testing, and critical interpretation of results are necessary for future advancements.~~

5 Conclusions

~~This study presents different techniques~~ Our study demonstrated the capability of metal oxide sensors to be used with flux algorithms to estimate emission rate and location during a controlled CH_4 release experiment, with release rates typical of those expected from gas leaks from industrial facilities. Our TGS voltage baseline correction algorithm allowed us to identify TGS voltage variations related to the high frequency variation of the plume across the different sensor inlets. We compared the performances of two models, 2nd degree polynomials and MLP, to reconstruct CH_4 mole fractions from ~~the voltage signal measured by metal oxide low cost TGS sensors deployed downwind an area of points of controlled releases during a campaign at TADI in 2019. The data from this reconstruction are assimilated in an inverse modelling framework to quantify the rate (ranging from 0.4 to 5 g CH~~voltage drop measurements during the controlled releases for three configurations of data from TGS units as inputs for the reconstruction algorithm. The reconstructed CH_4 ~~s^{-1}) and location of these controlled release . The approach employed to extract the baseline signal on TGS voltage measurementsbased on surrounding observations allowed us to derive and successfully correct the baseline signal on TGS sensors without the need of using other environmental parameters.~~ mole fractions were used as input to an inversion modelling framework for emission localisation and flux quantification for each release not otherwise used for model training (*i.e.* the testing data subset). Results of inversions assimilating reconstructed TGS mole fraction were compared with those assimilating corresponding reference (CRDS) mole fraction measurements.

The reconstruction of CH_4 mole fraction from voltage ~~observations measured~~ measurements made during controlled releases showed good agreement with ~~observed CH_4 mole fractions from the reference instruments~~corresponding measurements made by high-precision reference gas analysers. The reconstruction was consistently better ~~with~~ using data from the TGS 2611-C00 ~~sensor regardless~~ regardless of the reconstruction model used. Both ~~models had met our requirement target of NRMSE of reconstructed CH~~CH_4 mole fraction reconstruction models satisfied our targeted NRMSE requirement of lower than 0.15 ~~ppm across all chambers~~for all chambers, when trained with the TGS 2611-C00~~sensor~~. Emission rate and source location estimates using an inversion based on a gaussian plume model produced similar results using reconstructed CH_4 mole fraction derived from TGS sensors ~~data~~ to those obtained ~~with high precision instruments~~using high precision measurements, with an average ~~estimate~~ estimated TGS emission rate error of 25.5 % and a mean source location error of 9.5 m~~from TGS data~~. In this study, the reconstruction of the CH_4 mole fractions was conducted independently ~~from the~~ of inversion modelling. The emission flux estimation error could probably be reduced with a better understanding of inverse modelling sensitivity to the misfits from the reconstruction models. In consequence, a sensitivity study is encouraged in future to determine the best approach for the reconstruction ~~of the observations from TGS sensors~~TGS-derived methane mole fraction.

Data availability. The dataset was collected in the frame of the Chaire Indutrielle TRACE ANR-17-CHIN-0004-01. It is publicly accessible at this link: https://doi.org/10.5281/zenodo.8399829

Code availability. The codes developed in the frame of the Chaire Indutrielle TRACE ANR-17-CHIN-0004-01. They are accessible upon request to the corresponding author.

Appendix A: Models employed in the reconstruction of CH_4 concentrations from TGS voltage measurements

Second-degree polynomials proven to be robust to derive relationships between TGS voltage signal related to spikes and CH_4 mole fraction (Rivera Martinez et al., 2022), are defined by:

$$\hat{y}_{CH_4}(x_1) = \beta_0 + \beta_1 x_1 + \beta_2 x_1^2 \tag{A1}$$

Where $\hat{y}_{CH_4}$ is the predicted CH_4 concentration, x_1 is the Corrected voltage of the TGS after removing the effects of the baseline.

Artificial neural networks have been widely used to derive non-linear relationships between predictors and independent variables in many applications, as a universal approximator method (Hornik et al., 1989) and for their generalisation capabilities (Haykin, 1998). In previous studies (Casey et al., 2019; Eugster et al., 2020; Rivera Martinez et al., 2021, 2022), ANN was employed to derive CH_4 mole fractions from TGS observations on different sampling configurations (field and laboratory conditions) with good agreement between the reference observations and the outputs produced from the models. The simplest architecture of an ANN is the multi-layer perceptron (MLP), consisting of a series of units (neurons) in fully connected layers. The inputs of any unit will be the weighted sum of the outputs of the previous layer, to which an activation function (ReLU, tanh, etc.) is applied. As a supervised machine learning approach, it requires a training basis to learn the relationships, adjusting the weights of its connections, between the inputs and outputs using an iterative process known as optimization. Problems of MLP models are either underfit of data, producing a high error on the train set which can be mitigated with a sufficiently large network, or overfitting, producing a high test error when they cannot generalise to new examples. Regularisation terms and early stopping techniques are helpful to prevent overfitting (Bishop, 1995; Goodfellow et al., 2016). Here, we have trained the MLP model using the Adam optimizer (Kingma and Ba, 2014; Géron, 2019), and the optimal number of units and layers was determined using a grid search technique Géron (2019) resulting in 50, 10 and 5 units per layer with ReLU as the activation function for the hidden units. A regularisation factor of α = 0.05 and early stopping was used to prevent overfitting.

Author contributions. Olivier Laurent and Ford Cropley designed the Figaro® logger system. Olivier Laurent, Christopher Caldow and Ford Cropley conducted the field measurement campaign. Rodrigo Rivera and Diego Santaren developed the CH_4 reconstruction models. Rodrigo Rivera, Olivier Laurent and Cécile Mallet developed the baseline correction methodology of TGS sensors. Pramod Kumar and Rodrigo Rivera developed the inversion framework to estimate the release locations and emission rates. Rodrigo Rivera, Gregoire Broquet and Philippe Ciais prepared the manuscript with collaboration of the other co-authors.

Competing interests. The authors declare that they have no conflict of interest.

Acknowledgements. This work was supported by the Chaire Industrielle Trace ANR-17-CHIN-0004-01 co-funded by the ANR French national research agency, Total Energies-Raffinage Chimie, SUEZ - Smart & Environmental Solutions and THALES ALENIA SPACE.

References

Alvarez, R. A., Zavala-Araiza, D., Lyon, D. R., Allen, D. T., Barkley, Z. R., Brandt, A. R., Davis, K. J., Herndon, S. C., Jacob, D. J., Karion, A., Kort, E. A., Lamb, B. K., Lauvaux, T., Maasakkers, J. D., Marchese, A. J., Omara, M., Pacala, S. W., Peischl, J., Robinson, A. L., Shepson, P. B., Sweeney, C., Townsend-Small, A., Wofsy, S. C., and Hamburg, S. P.: Assessment of methane emissions from the U.S. oil and gas supply chain, Science, p. eaar7204, https://doi.org/10.1126/science.aar7204, 2018.

Bastviken, D., Nygren, J., Schenk, J., Parellada Massana, R., and Duc, N. T.: Technical note: Facilitating the use of low-cost methane (CH_4) sensors in flux chambers – calibration, data processing, and an open-source make-it-yourself logger, Biogeosciences, 17, 3659–3667, https://doi.org/10.5194/bg-17-3659-2020, 2020.

Bell, C., Ilonze, C., Duggan, A., and Zimmerle, D.: Performance of Continuous Emission Monitoring Solutions under a Single-Blind Controlled Testing Protocol, Environmental Science & Technology, 57, 5794–5805, https://doi.org/10.1021/acs.est.2c09235, pMID: 36977200, 2023.

Bishop, C. M.: Neural Networks for Pattern Recognition, Oxford University Press, Inc., 1995.

Casey, J. G., Collier-Oxandale, A., and Hannigan, M.: Performance of artificial neural networks and linear models to quantify 4 trace gas species in an oil and gas production region with low-cost sensors, Sensors and Actuators B: Chemical, 283, https://doi.org/10.1016/j.snb.2018.12.049, 2019.

Chamberland, J.-F. and Veeravalli, V.: How Dense Should a Sensor Network Be for Detection With Correlated Observations?, IEEE Transactions on Information Theory, 52, 5099–5106, https://doi.org/10.1109/TIT.2006.883551, 2006.

Collier-Oxandale, A., Casey, J. G., Piedrahita, R., Ortega, J., Halliday, H., Johnston, J., and Hannigan, M. P.: Assessing a low-cost methane sensor quantification system for use in complex rural and urban environments, Atmospheric Measurement Techniques, 11, https://doi.org/10.5194/amt-11-3569-2018, 2018.

Collier-Oxandale, A. M., Thorson, J., Halliday, H., Milford, J., and Hannigan, M.: Understanding the ability of low-cost MOx sensors to quantify ambient VOCs, Atmospheric Measurement Techniques, 12, https://doi.org/10.5194/amt-12-1441-2019, 2019.

Eugster, W. and Kling, G. W.: Performance of a low-cost methane sensor for ambient concentration measurements in preliminary studies, Atmospheric Measurement Techniques, 5, https://doi.org/10.5194/amt-5-1925-2012, 2012.

Eugster, W., Laundre, J., Eugster, J., and Kling, G. W.: Long-term reliability of the Figaro TGS 2600 solid-state methane sensor under low-Arctic conditions at Toolik Lake, Alaska, Atmospheric Measurement Techniques, 13, https://doi.org/10.5194/amt-13-2681-2020, 2020.

Figaro®: Figaro (2005), https://www.figaro.co.jp/en/product/entry/tgs2600.html, accessed on 10 February 2020 accessed on 10 February 2020, 2005.

Figaro®: Figaro (2013), https://www.figaro.co.jp/en/product/entry/tgs2611-c00.html, accessed on 10 February 2020, 2013.

Goodfellow, I., Bengio, Y., and Courville, A.: Deep Learning, MIT Press, http://www.deeplearningbook.org, 2016.

Géron, A.: Hands-on machine learning with Scikit-Learn, Keras, and TensorFlow: Concepts, tools, and techniques to build intelligent systems, O'Reilly Media, 2019.

Haykin, S.: Neural Networks: A Comprehensive Foundation, Prentice Hall PTR, 2nd edn., 1998.

Hornik, K., Stinchcombe, M., and White, H.: Multilayer feedforward networks are universal approximators, Neural Networks, 2, https://doi.org/10.1016/0893-6080(89)90020-8, 1989.

Kingma, D. P. and Ba, J.: Adam: A method for stochastic optimization, arXiv preprint arXiv:1412.6980, 2014.

Kumar, P., Morawska, L., Martani, C., Biskos, G., Neophytou, M., Sabatino, S. D., Bell, M., Norford, L., and Britter, R.: The rise of low-cost sensing for managing air pollution in cities, Environment International, 75, https://doi.org/10.1016/j.envint.2014.11.019, 2015.

Kumar, P., Broquet, G., Yver-Kwok, C., Laurent, O., Gichuki, S., Caldow, C., Cropley, F., Lauvaux, T., Ramonet, M., Berthe, G., Martin, F., Duclaux, O., Juery, C., Bouchet, C., and Ciais, P.: Mobile atmospheric measurements and local-scale inverse estimation of the location and rates of brief $CH_{\{4\}}$ and $CO_{\{2\}}$ releases from point sources, Atmospheric Measurement Techniques, 14, 5987–6003, https://doi.org/10.5194/amt-14-5987-2021, 2021.

Kumar, P., Broquet, G., Caldow, C., Laurent, O., Gichuki, S., Cropley, F., Yver-Kwok, C., Fontanier, B., Lauvaux, T., Ramonet, M., Shah, A., Berthe, G., Martin, F., Duclaux, O., Juery, C., Bouchet, C., Pitt, J., and Ciais, P.: Near-field atmospheric inversions for the localization and quantification of controlled methane releases using stationary and mobile measurements, Quarterly Journal of the Royal Meteorological Society, https://doi.org/10.1002/qj.4283, 2022.

Mead, M., Popoola, O., Stewart, G., Landshoff, P., Calleja, M., Hayes, M., Baldovi, J., McLeod, M., Hodgson, T., Dicks, J., Lewis, A., Cohen, J., Baron, R., Saffell, J., and Jones, R.: The use of electrochemical sensors for monitoring urban air quality in low-cost, high-density networks, Atmospheric Environment, 70, 186–203, https://doi.org/10.1016/j.atmosenv.2012.11.060, 2013.

Picarro Inc.: Santa Clara, CA, USA: .

Popoola, O. A., Carruthers, D., Lad, C., Bright, V. B., Mead, M. I., Stettler, M. E., Saffell, J. R., and Jones, R. L.: Use of networks of low cost air quality sensors to quantify air quality in urban settings, Atmospheric Environment, 194, https://doi.org/10.1016/j.atmosenv.2018.09.030, 2018.

Riddick, S. N., Mauzerall, D. L., Celia, M., Allen, G., Pitt, J., Kang, M., and Riddick, J. C.: The calibration and deployment of a low-cost methane sensor, Atmospheric Environment, 230, 117 440, https://doi.org/10.1016/j.atmosenv.2020.117440, 2020.

Riddick, S. N., Ancona, R., Cheptonui, F., Bell, C. S., Duggan, A., Bennett, K. E., and Zimmerle, D. J.: A cautionary report of calculating methane emissions using low-cost fence-line sensors, Elementa: Science of the Anthropocene, 10, 00 021, https://doi.org/10.1525/elementa.2022.00021, 2022.

Rivera Martinez, R., Santaren, D., Laurent, O., Cropley, F., Mallet, C., Ramonet, M., Caldow, C., Rivier, L., Broquet, G., Bouchet, C., Juery, C., and Ciais, P.: The Potential of Low-Cost Tin-Oxide Sensors Combined with Machine Learning for Estimating Atmospheric CH4 Variations around Background Concentration, Atmosphere, 12, https://doi.org/10.3390/atmos12010107, 2021.

Rivera Martinez, R. A., Santaren, D., Laurent, O., Broquet, G., Cropley, F., Mallet, C., Ramonet, M., Shah, A., Rivier, L., Bouchet, C., Juery, C., Duclaux, O., and Ciais, P.: Reconstruction of high-frequency methane atmospheric concentration peaks from measurements using metal oxide low-cost sensors, Atmospheric Measurement Techniques Discussions, 2022, 1–45, https://doi.org/10.5194/amt-2022-200, 2022.

Saunois, M., Stavert, A. R., Poulter, B., Bousquet, P., Canadell, J. G., Jackson, R. B., Raymond, P. A., Dlugokencky, E. J., Houweling, S., Patra, P. K., Ciais, P., Arora, V. K., Bastviken, D., Bergamaschi, P., Blake, D. R., Brailsford, G., Bruhwiler, L., Carlson, K. M., Carrol, M., Castaldi, S., Chandra, N., Crevoisier, C., Crill, P. M., Covey, K., Curry, C. L., Etiope, G., Frankenberg, C., Gedney, N., Hegglin, M. I., Höglund-Isaksson, L., Hugelius, G., Ishizawa, M., Ito, A., Janssens-Maenhout, G., Jensen, K. M., Joos, F., Kleinen, T., Krummel, P. B., Langenfelds, R. L., Laruelle, G. G., Liu, L., Machida, T., Maksyutov, S., McDonald, K. C., McNorton, J., Miller, P. A., Melton, J. R., Morino, I., Müller, J., Murguia-Flores, F., Naik, V., Niwa, Y., Noce, S., O'Doherty, S., Parker, R. J., Peng, C., Peng, S., Peters, G. P., Prigent, C., Prinn, R., Ramonet, M., Regnier, P., Riley, W. J., Rosentreter, J. A., Segers, A., Simpson, I. J., Shi, H., Smith, S. J., Steele, L. P., Thornton, B. F., Tian, H., Tohjima, Y., Tubiello, F. N., Tsuruta, A., Viovy, N., Voulgarakis, A., Weber, T. S., van Weele, M., van der Werf, G. R., Weiss, R. F., Worthy, D., Wunch, D., Yin, Y., Yoshida, Y., Zhang, W., Zhang, Z., Zhao, Y., Zheng, B., Zhu, Q., Zhu, Q., and Zhuang,

Q.: The Global Methane Budget 2000–2017, Earth System Science Data, 12, 1561–1623, https://doi.org/10.5194/essd-12-1561-2020, 2020.

Shah, A., Laurent, O., Lienhardt, L., Broquet, G., Rivera Martinez, R., Allegrini, E., and Ciais, P.: Characterising the methane gas and environmental response of the figaro taguchi gas sensor (TGS) 2611-E00, Atmospheric Measurement Techniques, 16, 3391–3419, https://doi.org/10.5194/amt-16-3391-2023, publisher: Copernicus GmbH, 2023.

Shah, A., Laurent, O., Broquet, G., Philippon, C., Kumar, P., Allegrini, E., and Ciais, P.: Determining methane mole fraction at a landfill site using the figaro taguchi gas sensor 2611-C00 and wind direction measurements, Environmental Science: Atmospheres, 4, 362–386, https://doi.org/10.1039/D3EA00138E, 2024.

Singh, S. K., Sharan, M., and Issartel, J.-P.: Inverse modelling for identification of multiple-point releases from atmospheric concentration measurements, Boundary-Layer Meteorology, 146, 277–295, https://doi.org/10.1007/s10546-012-9765-y, 2013.

Travis, B., Dubey, M., and Sauer, J.: Neural networks to locate and quantify fugitive natural gas leaks for a MIR detection system, Atmospheric Environment: X, 8, 100 092, https://doi.org/10.1016/j.aeaoa.2020.100092, 2020.

van den Bossche, M., Rose, N. T., and De Wekker, S. F. J.: Potential of a low-cost gas sensor for atmospheric methane monitoring, Sensors and Actuators B: Chemical, 238, 501–509, https://doi.org/https://doi.org/10.1016/j.snb.2016.07.092, 2017.

Yver-Kwok, C., Laurent, O., Guemri, A., Philippon, C., Wastine, B., Rella, C. W., Vuillemin, C., Truong, F., Delmotte, M., Kazan, V., Darding, M., Lebègue, B., Kaiser, C., Xueref-Rémy, I., and Ramonet, M.: Comprehensive laboratory and field testing of cavity ring-down spectroscopy analyzers measuring H_2O, CO_2, CH_4 and CO, Atmospheric Measurement Techniques, 8, 3867–3892, https://doi.org/10.5194/amt-8-3867-2015, 2015.

Özgür Örnek and Karlik, B.: An overview of metal oxide semiconducting sensors in electronic nose applications, vol. 2, pp. 506–515, 2012.

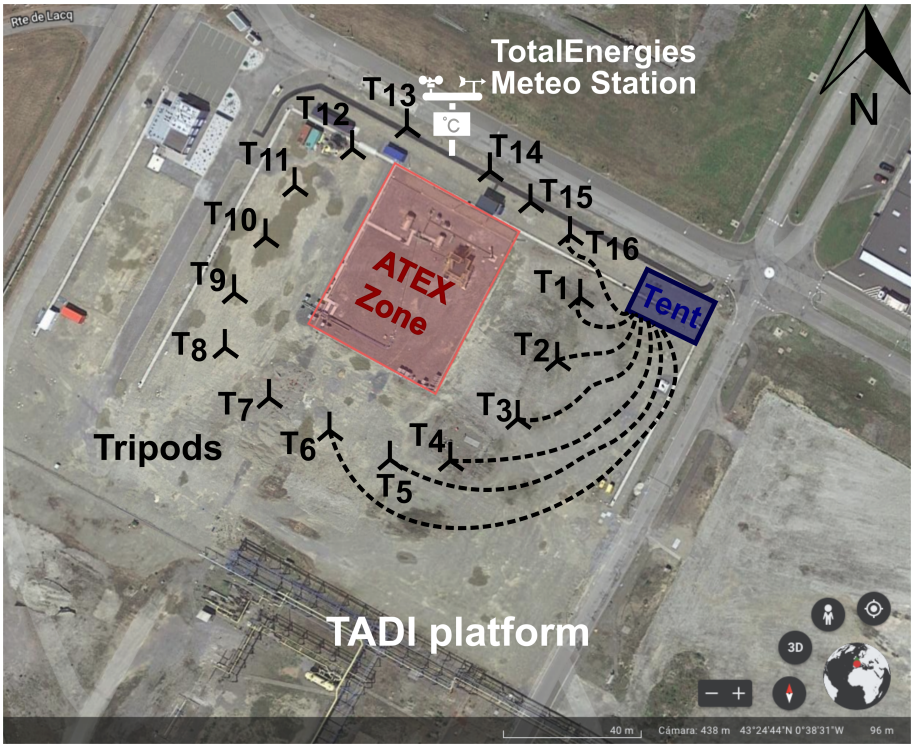

Figure 1. Diagram of the experimental setup on top of a satellite image of the TADI platform (source: Google Earth©). The locations of the releases are inside the red rectangle (ATEX zone). The locations of the 16 tripods are presented as black symbols and denoted with a Tx where x is the index of the tripod from 1 to 16. The blue rectangle indicates the tent location. Examples of the sampling lines connecting the tripods to the tent are shown as dashed lines, only showing 7 of 16 in total. The white symbol shows the location of the Meteorological station installed by TotalEnergies® .

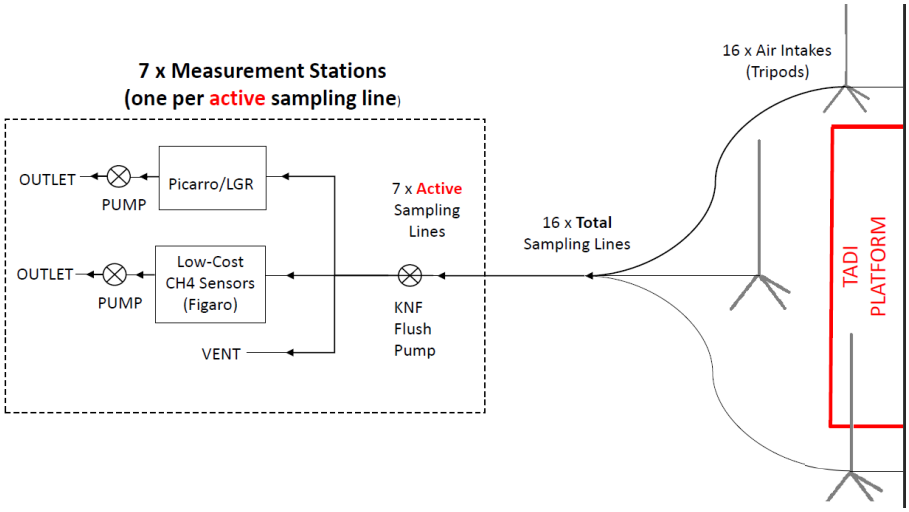

Figure 2. Diagram of the measurement stations and their connection to the sampling lines.

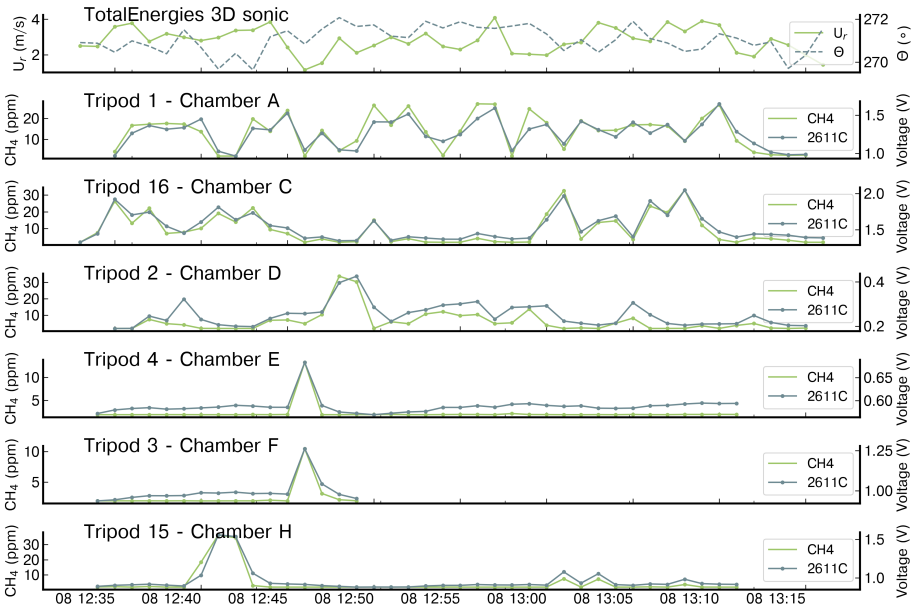

Figure 3. An example of 1-minute averaged ~~CH_4~~ CH4 mole fraction (ppm) and voltage drop (V) measurements, respectively~~measured by~~, obtained from six high precision instruments and one type of TGS sensor (TGS 2611-C00) for release 25 ($Q_s = 5$ g s^{-1}). CH_4 measurements from the high precision instruments are denoted as 'CH4' and the voltage measurements from TGS sensor are denoted as '2611C'. The top panel shows the 1-minute averaged wind speed (~~Ur~~U_r) and wind direction (θ) measured by the 3D sonic anemometer.

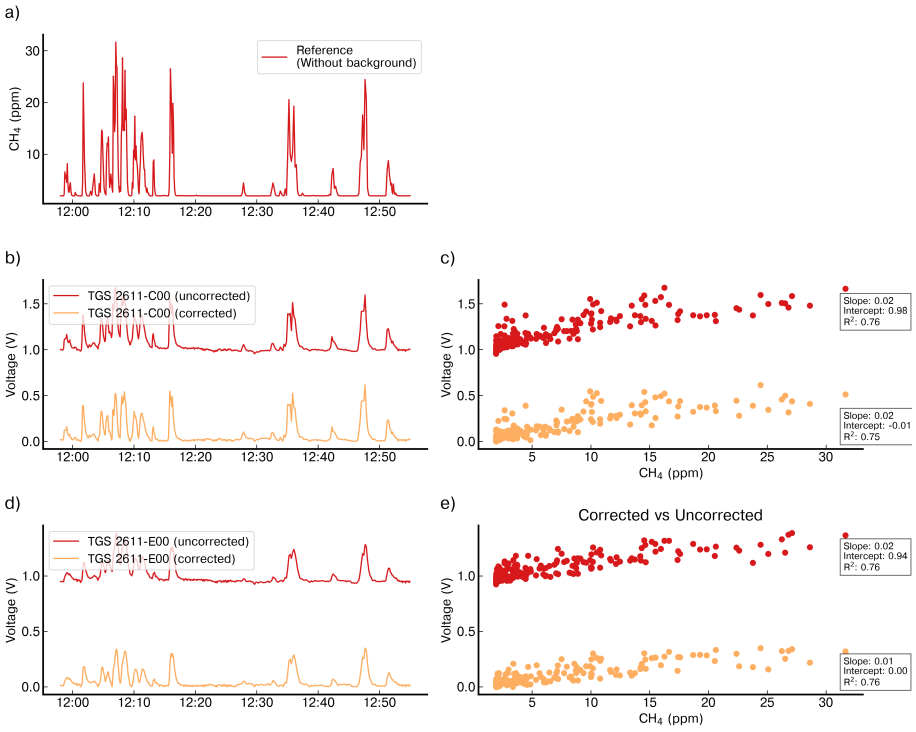

Figure 4. Comparison of the voltage signal for one release (#8) from Chamber A before (Uncorrected) and after (Corrected) the baseline correction on (b) TGS 2611-C00 and (~~e~~d) TGS 2611-E00, on which it is appreciated the correction of the offset preserving the amplitude enhancements linked to CH4 variations. Scatter plot of the corrected (orange) and uncorrected (red) signal vs the reference CH_4 ~~variations~~observations for (c) TGS 2611-C00 and (e) TGS 2611-E00. (a) Reference CH_4 mole fractions, also corrected using the spike correction algorithm.

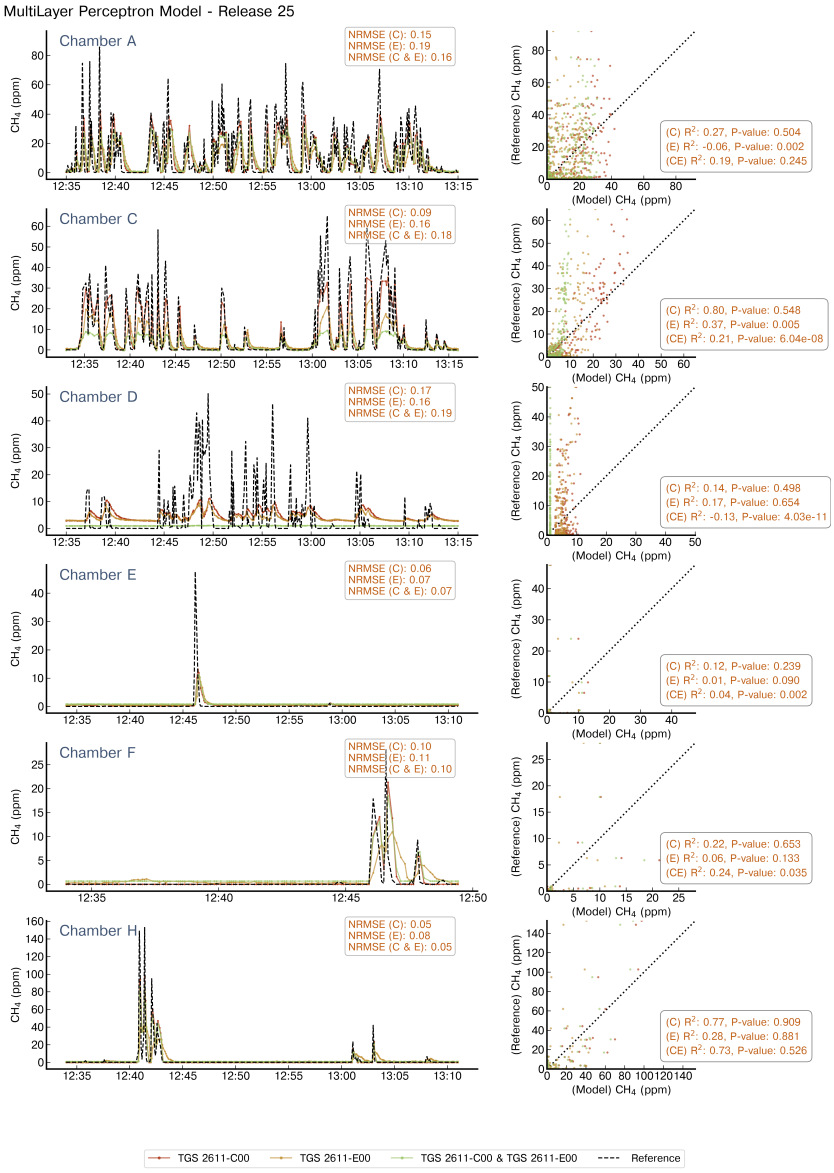

Figure 5. Example of reconstruction of release #25 using an MLP model. On left panels are shown the reconstructed CH_4 mole fractions for each chamber that captured the release, we present the reference signal (black dotted line), the reconstructed CH_4 mole fractions when the model has as input the TGS 2611-C00 sensor (red), the TGS 2611-E00 (yellow) or both types at the same time (green). The right panels show the 1:1 plot of the reference against the output of the model for the three configurations of inputs. Note the difference in the x-axis for Chamber F.

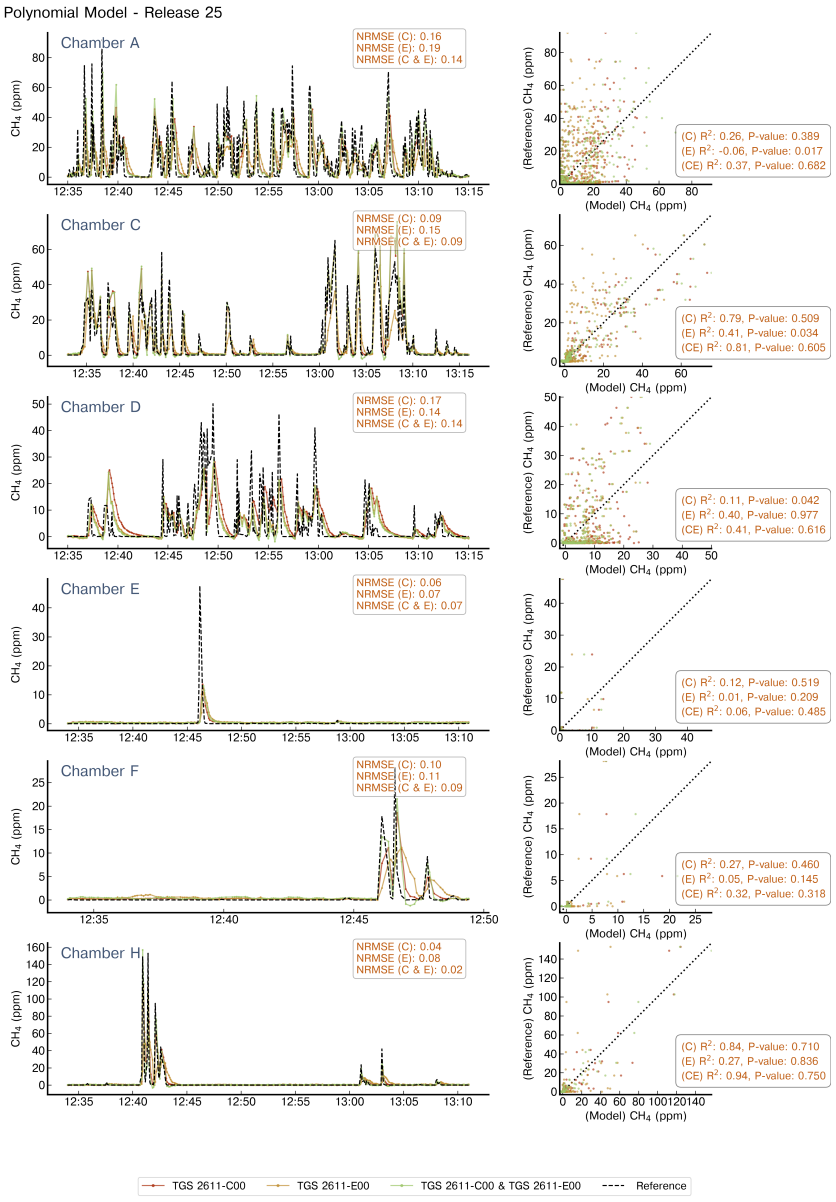

Figure 6. Example of reconstruction of release #25 using a Polynomial model. Notations are the same as in Figure 5.

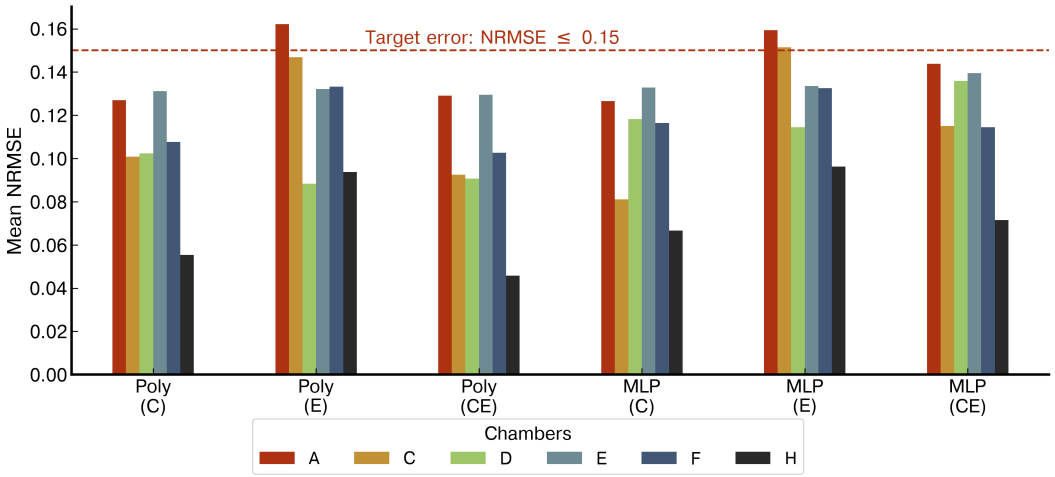

Figure 7. Comparison of the mean NRMSE of the two types of models trained with the three configurations of the inputs. The ~~2nd~~ 2nd degree polynomials are denoted as 'Poly' and the multilayer perceptron as 'MLP'. The three input configurations are denoted inside parentheses, 'C' when the model's input was only the TGS 2611-C00, 'E' for the TGS 2611-E00 and 'CE' when both sensors were used as inputs at the same time. The color code of the bars corresponds to the chambers.

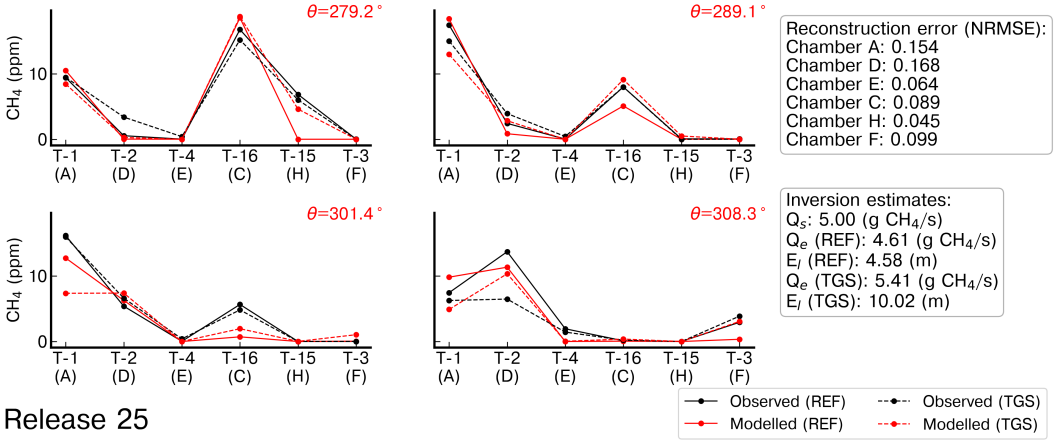

Figure 8. Observed and modelled average CH_4 mole fractions from the reference gas analyser, denoted 'REF', and ~~low-cost sensor~~TGS 2611-C00 sensors, denoted TGS, corresponding to ~~the~~ release #25. ~~The reconstructed~~ Reconstructed CH_4 ~~was~~ measurements were computed using the MLP model. The index of the ~~tripods~~ air inlets is denoted as T-x and the average wind direction (θ) for the binning of wind sectors is shown on the top right of each panel in red.

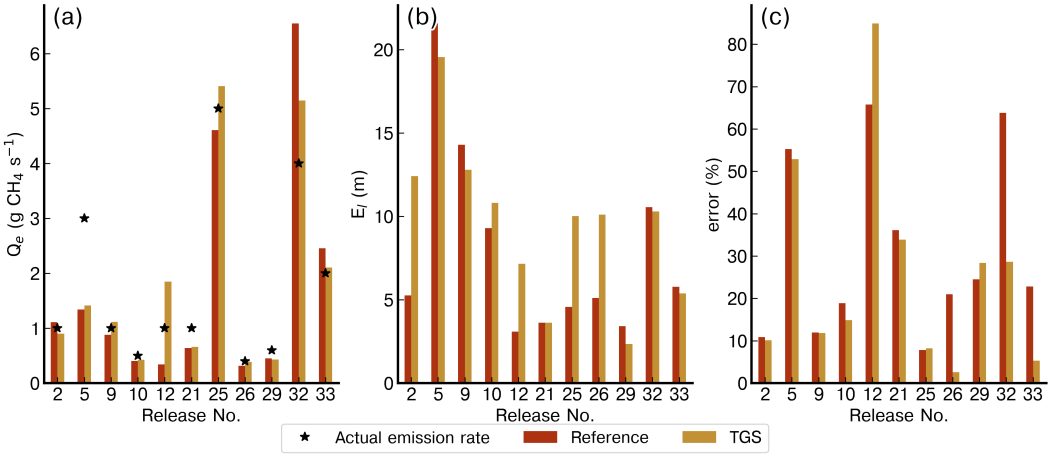

Figure 9. Comparison of the emission rate estimate (*Qe*) (a), of the location error (*El*) (b) and of the relative error in the emission rate estimate (c) from the inversions assimilating the Reference data (in red) and the reconstruction of the CH_4 mole fraction from the TGS sensors (in orange). The reconstructed CH_4 mole fractions used in these inversions are computed with the MLP model.

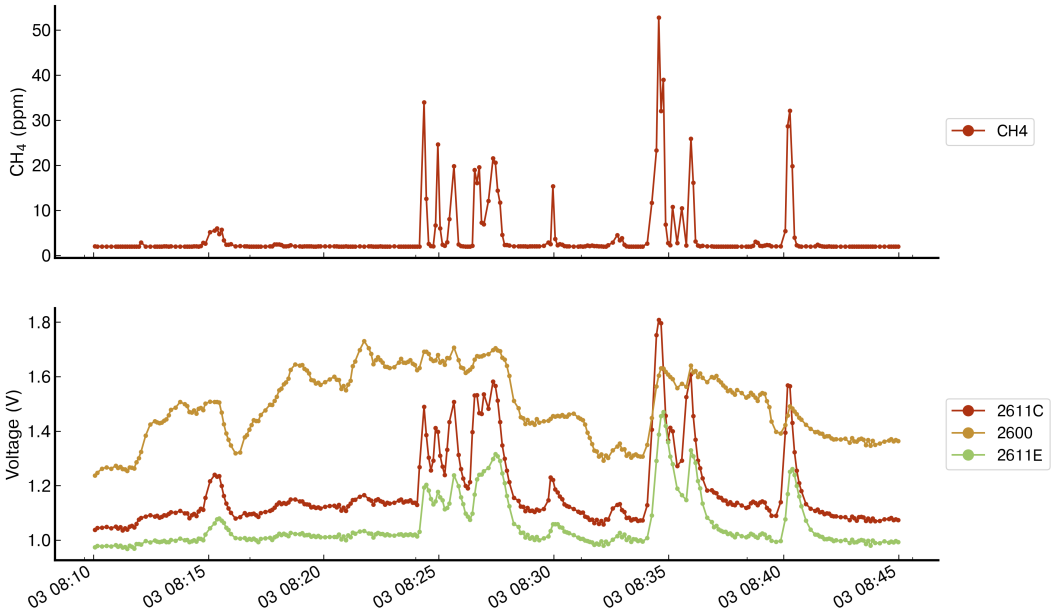

Figure A1. Comparison of the voltage measurements from three types of TGS included on chamber A. Upper plot shows the reference CH_4 observations measured from the reference instrument. Lower plot shows the voltage observations from TGS 2611-C00, 2600 and 2611-E00.

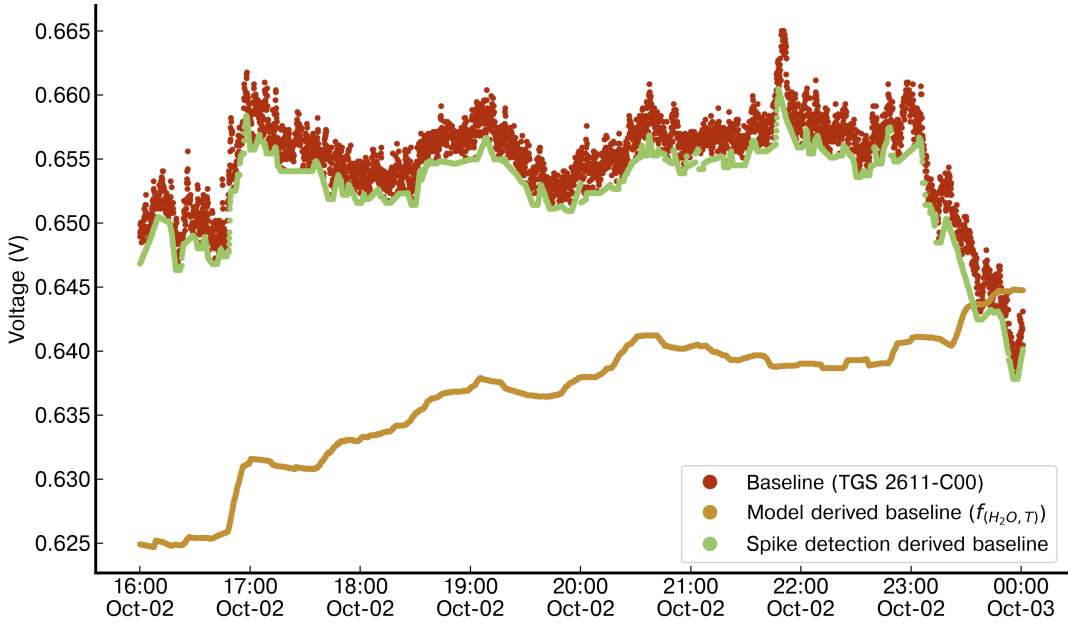

Figure A2. Comparison of the performance in deriving a baseline signal for the TGS 2611-C00 (red) of Chamber E between a function of H_2O and Temperature (yellow) and a spike detection algorithm (green). The multilinear model derived baseline was trained on six hours of non-release periods at the start of the first day of the campaign and evaluated on the last eight hours of the same day (shown in the figure). The Spike detection algorithm, an iterative function, does not need any prior training and detects the baseline based on ~~neighboring~~ neighbouring observations and fixed parameters.

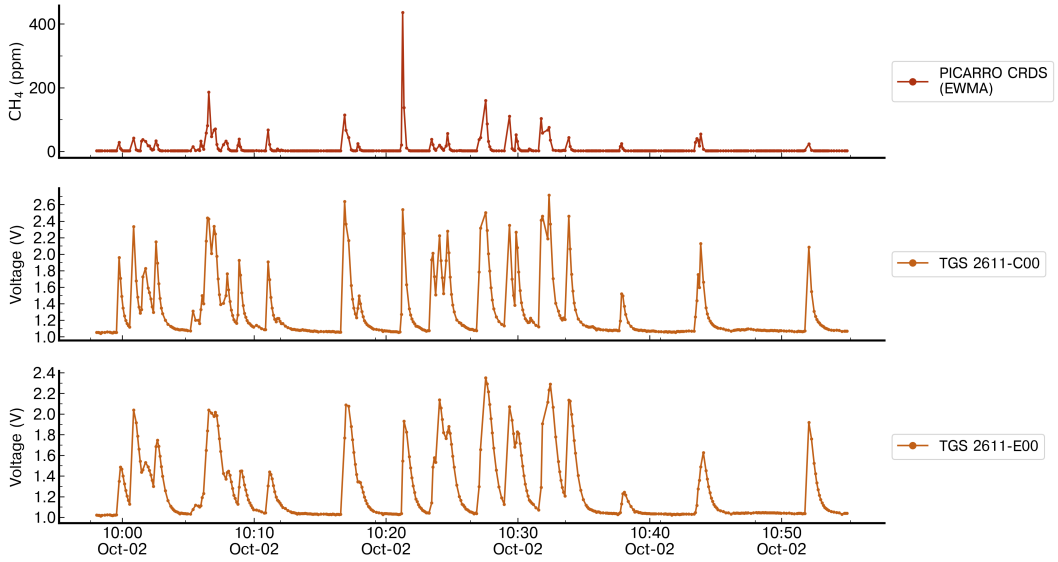

Figure A3. Comparison of the response of the TGS 2611-C00 and TGS 2611-E00 sensors with CH_4 measurements from the reference instrument for the release #2 which contains spikes with high concentration. The spikes observed on the TGS sensors corresponding from amplitudes between 100 ppm to more than 200 ppm are not distinguishable from spikes with amplitudes lower than 50 ppm.

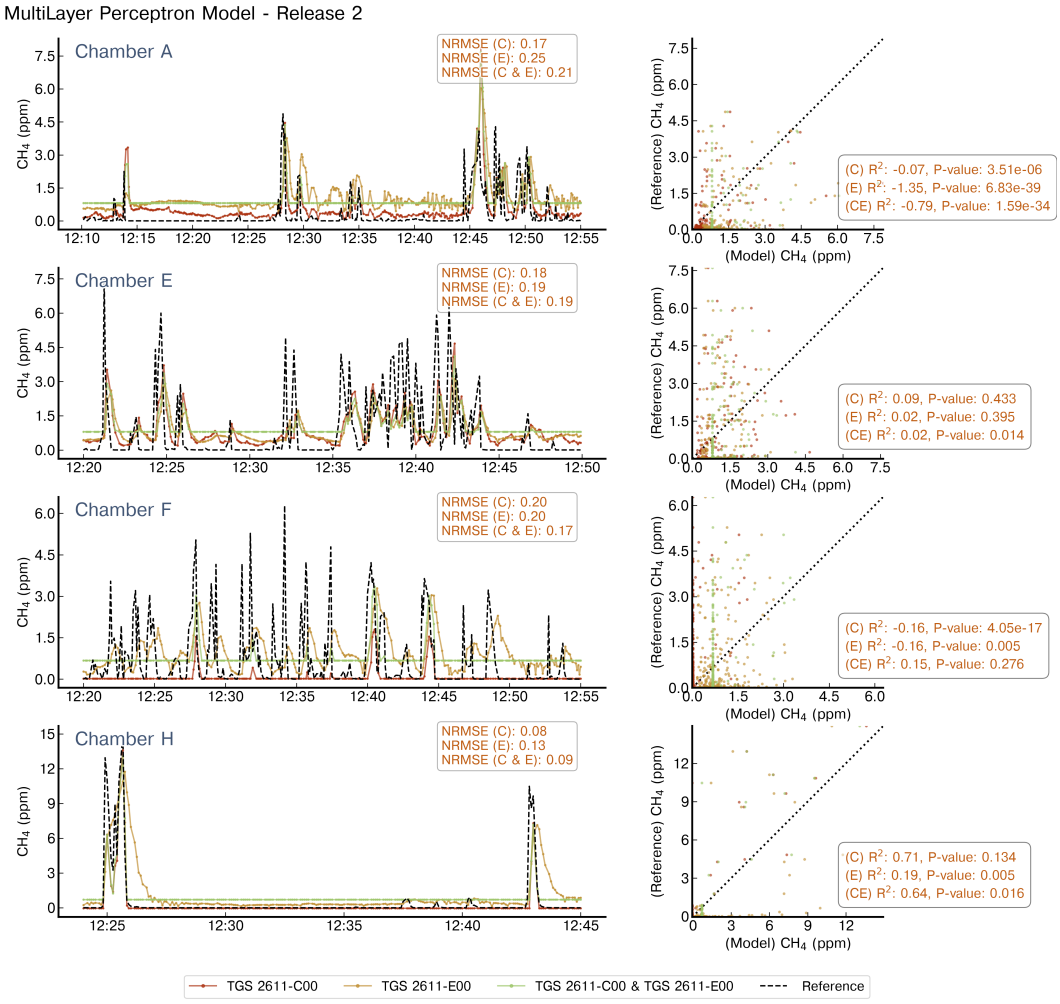

Figure A4. Reconstruction of release #2 using a MLP model. On left panels are shown the reconstructed CH_4 mole fractions for each chamber that captured the release, we present the reference signal (black dotted line), the reconstructed CH_4 mole fractions when the model has as input the TGS 2611-C00 sensor (red), the TGS 2611-E00 (yellow) or both types at the same time (green). The right panels show the 1:1 plot of the reference against the output of the model for the three configurations of inputs. Note the difference in the x-axis for the chambers.

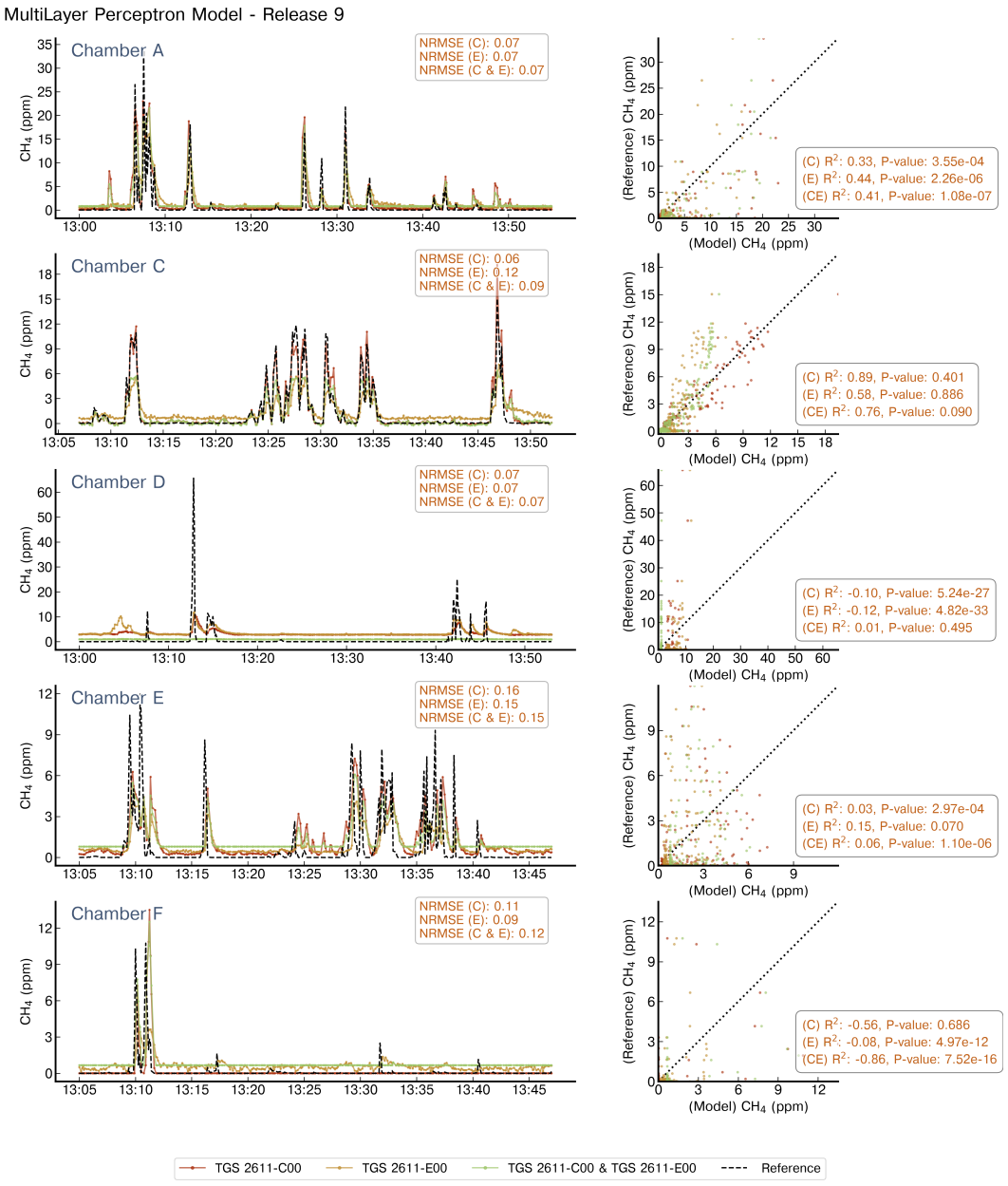

Figure A5. Reconstruction of release #9 using a MLP model. Notations are the same as in Figure A4. Note the difference in the x-axis for the chambers.

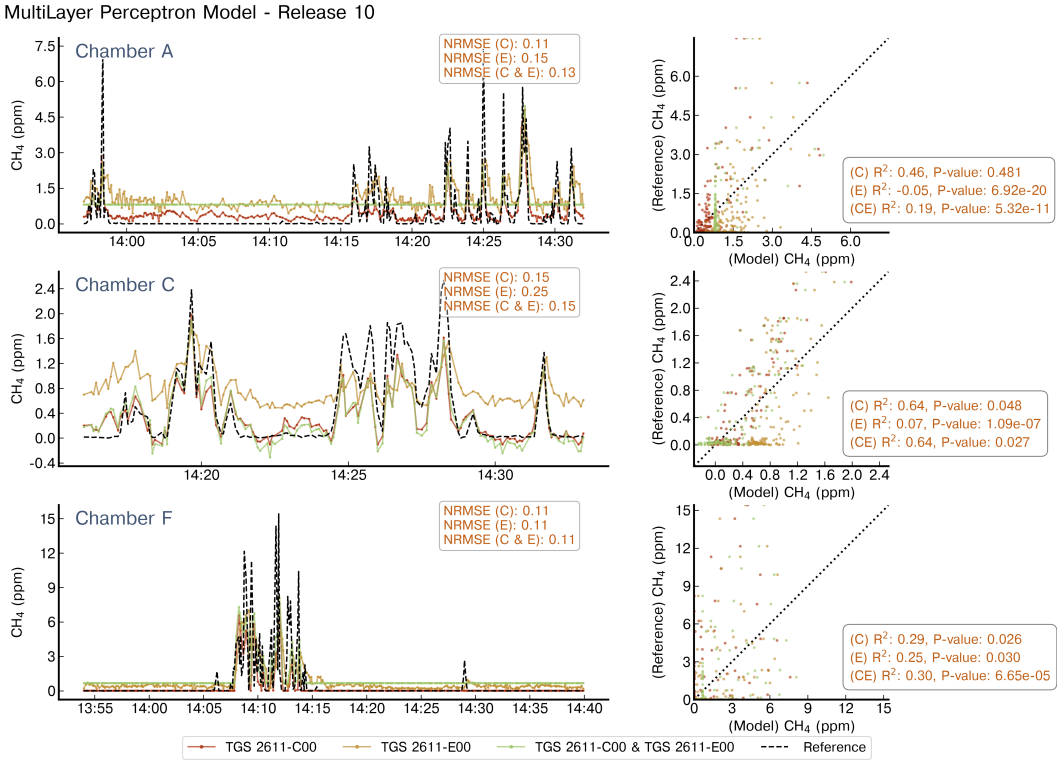

Figure A6. Reconstruction of release #10 using a MLP model. Notations are the same as in Figure A4. Note the difference in the x-axis for the chambers.

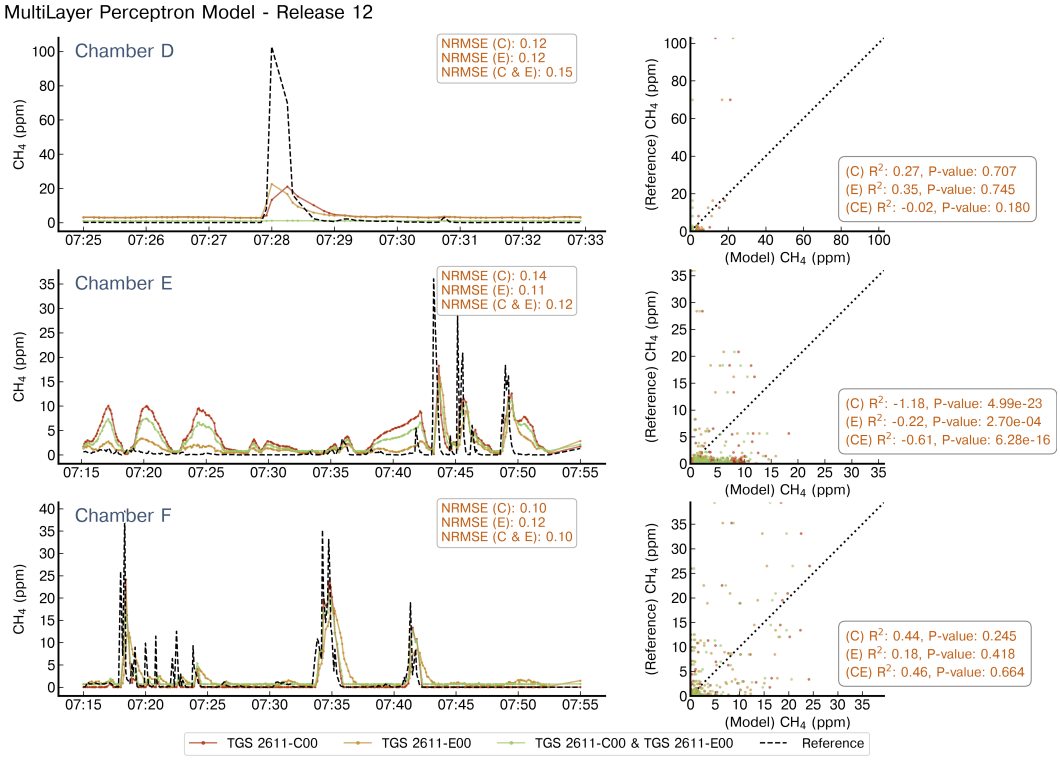

Figure A7. Reconstruction of release #12 using a MLP model. Notations are the same as in Figure A4. Note the difference in the x-axis for the chambers.

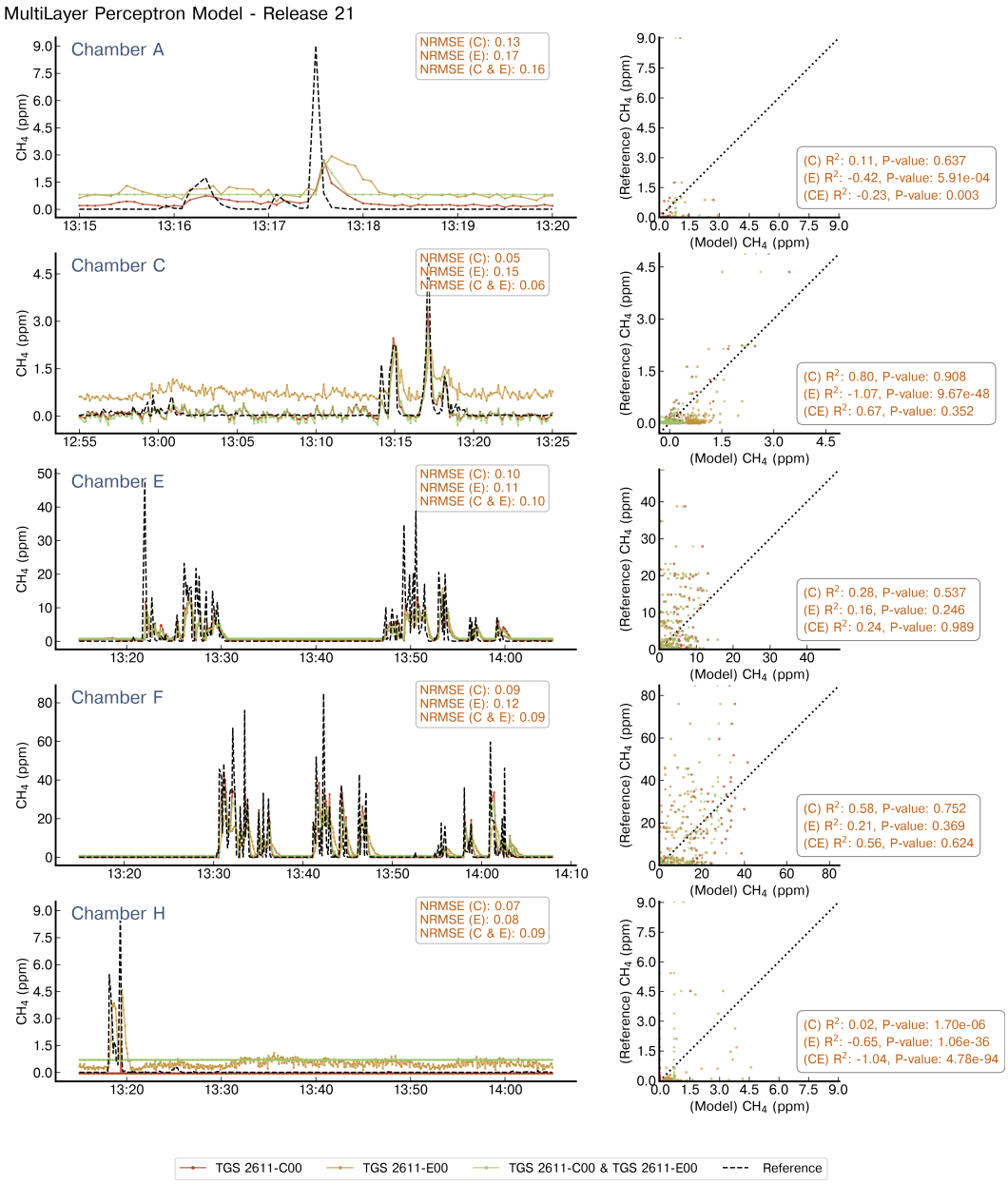

Figure A8. Reconstruction of release #21 using a MLP model. Notations are the same as in Figure A4. Note the difference in the x-axis for the chambers.

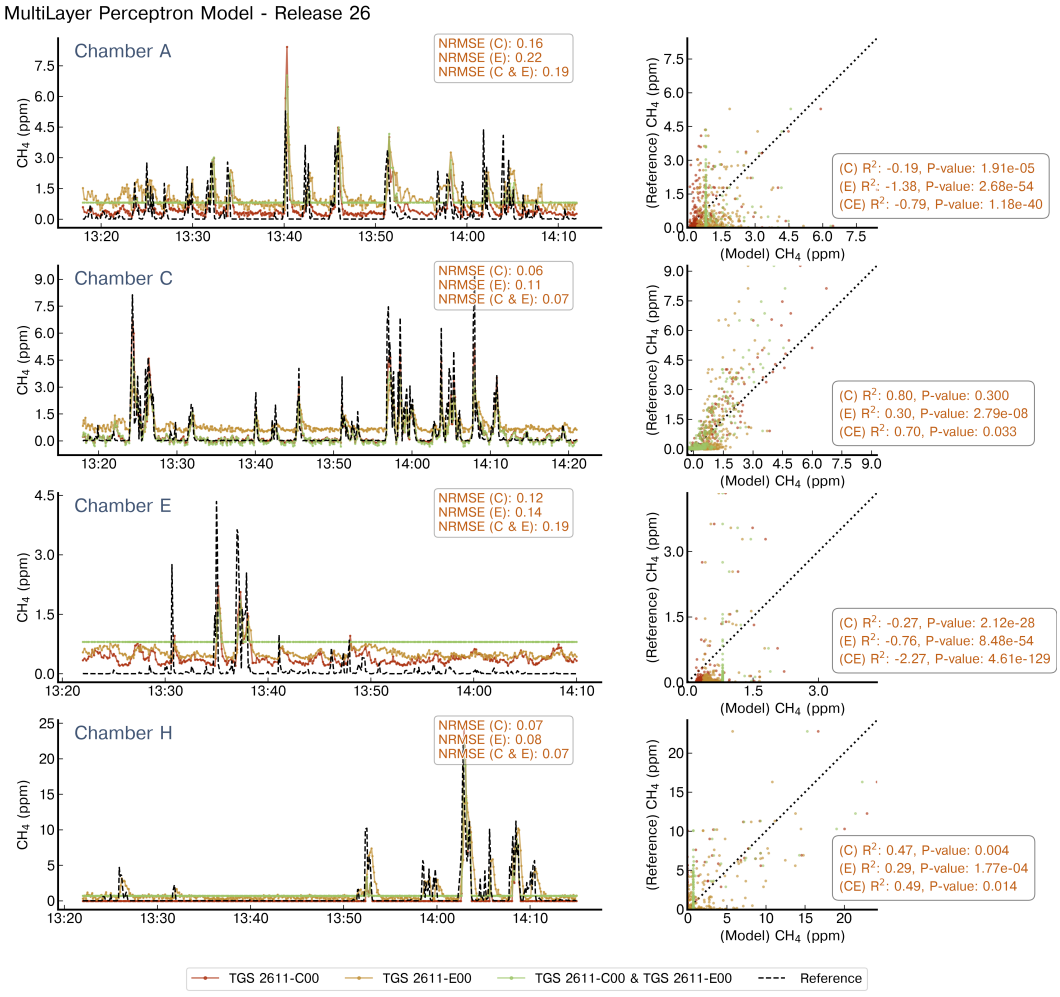

Figure A9. Reconstruction of release #26 using a MLP model. Notations are the same as in Figure A4. Note the difference in the x-axis for the chambers.

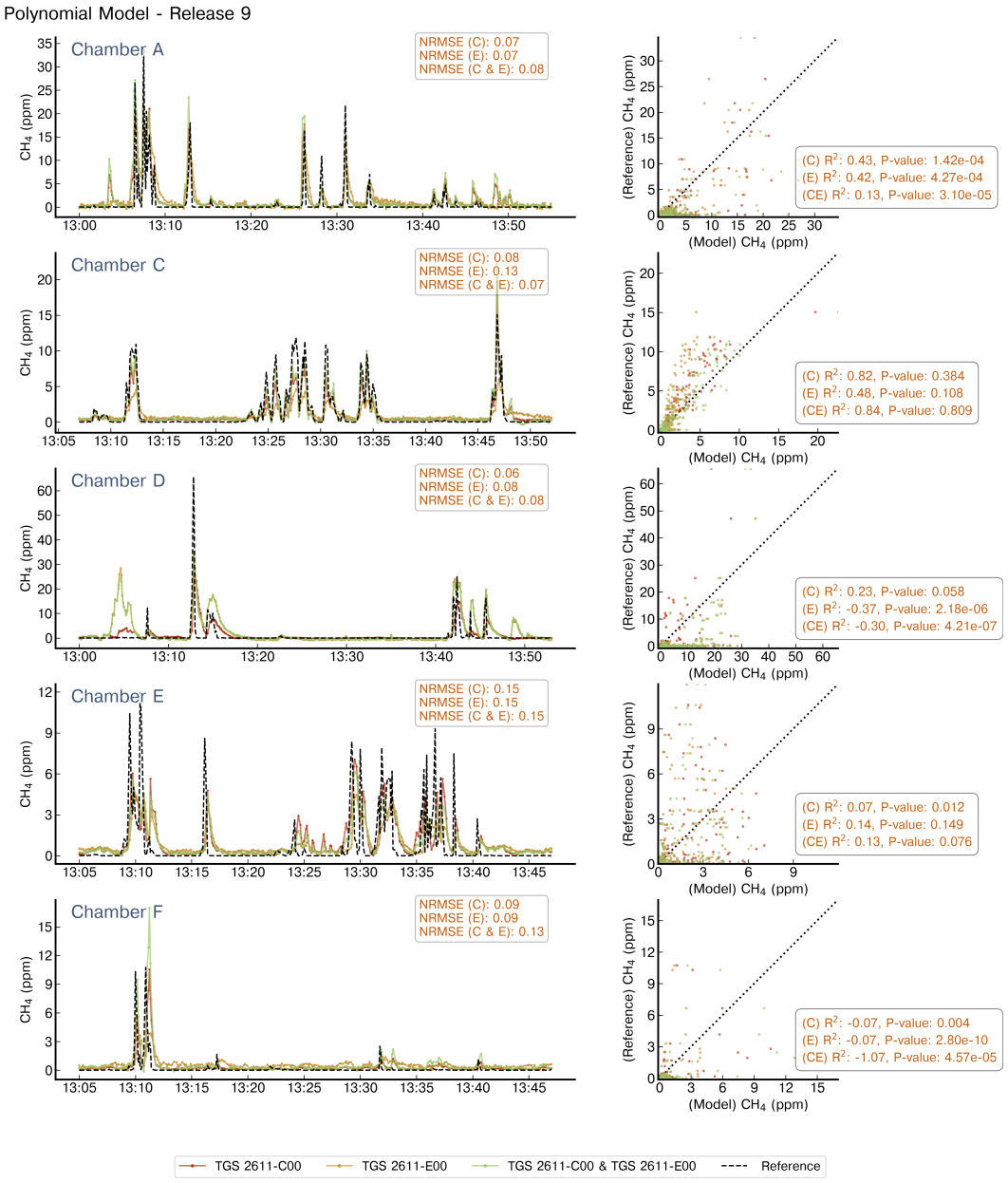

Figure A10. Reconstruction of release #9 using ~~2nd~~ 2nd degree polynomials. Notations are the same as in Figure A4. Note the difference in the x-axis for the chambers.

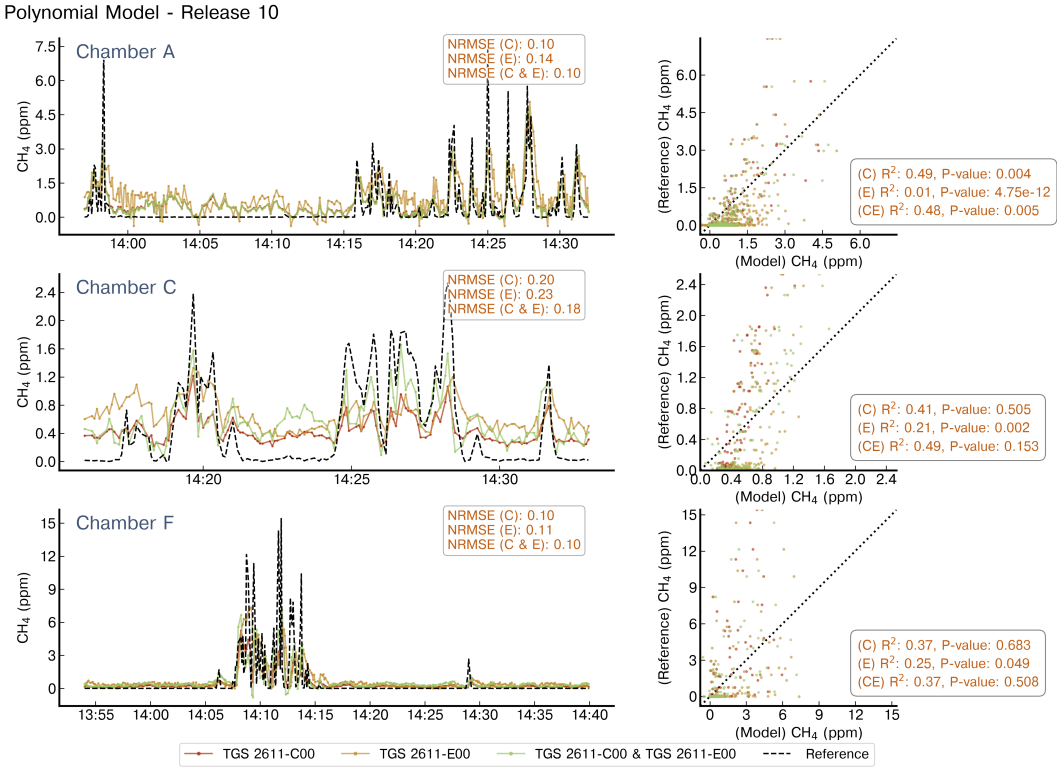

Figure A11. Reconstruction of release #10 using ~~2nd~~ 2nd degree polynomials. Notations are the same as in Figure A4. Note the difference in the x-axis for the chambers.

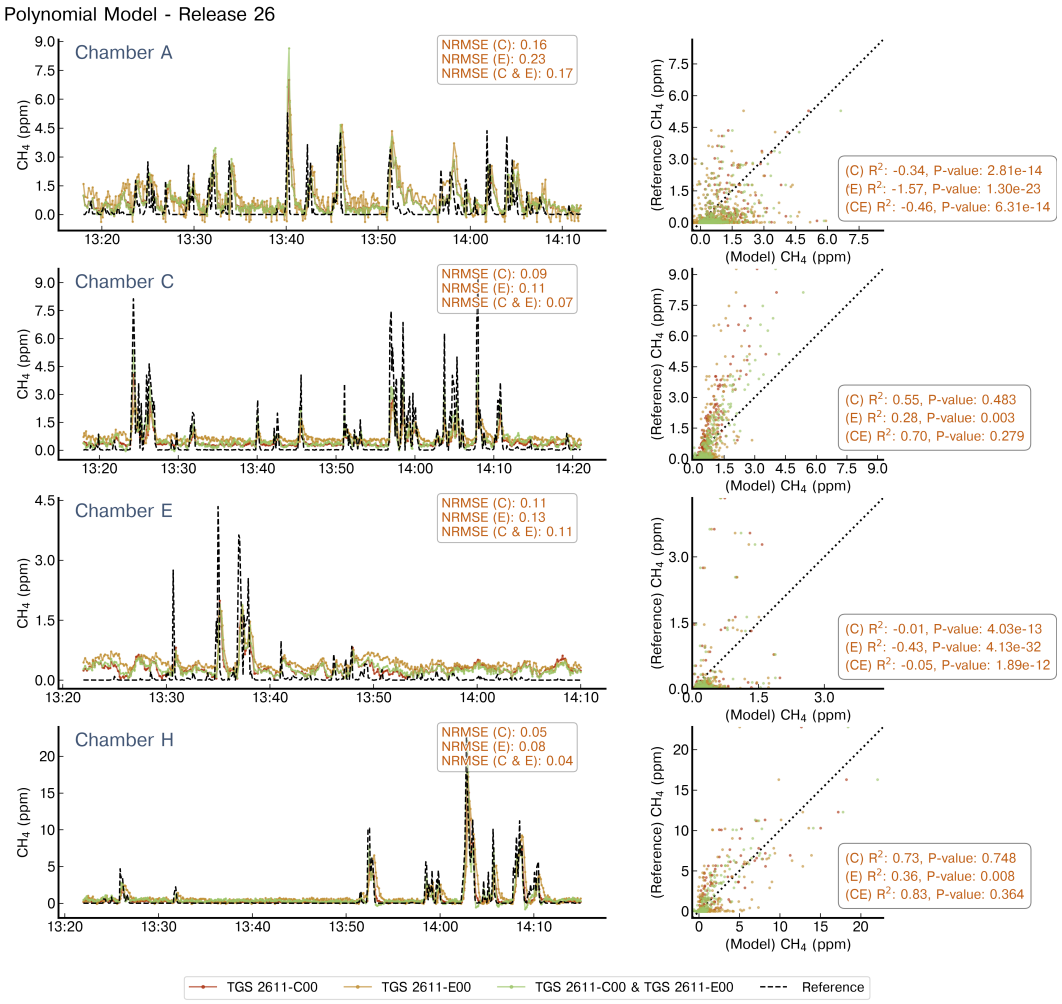

Figure A12. Reconstruction of release #26 using ~~2nd~~ 2nd degree polynomials. Notations are the same as in Figure A4. Note the difference in the x-axis for the chambers.

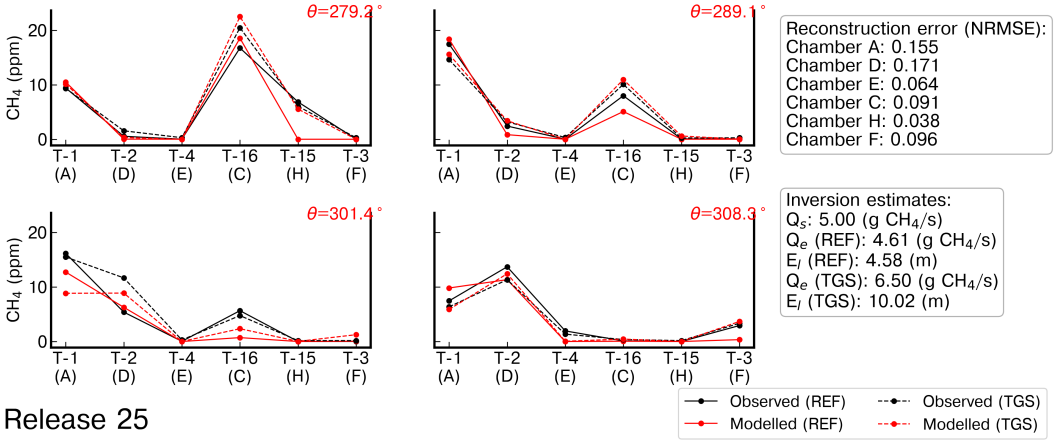

Figure A13. Observed and modelled average CH_4 mole fractions from the reference gas analyser, denoted 'REF', and ~~low-cost sensor~~TGS 2611-C00 sensors, denoted TGS, corresponding to ~~the~~ release #25. ~~The reconstructed~~ Reconstructed CH_4 ~~was~~ measurements were computed using the 2nd degree polynomial model~~of 2nd degree~~. The index of the ~~tripods~~ air inlets is denoted as T-x and the average wind direction (θ) for the binning of wind sectors is shown on the top right of each panel in red.

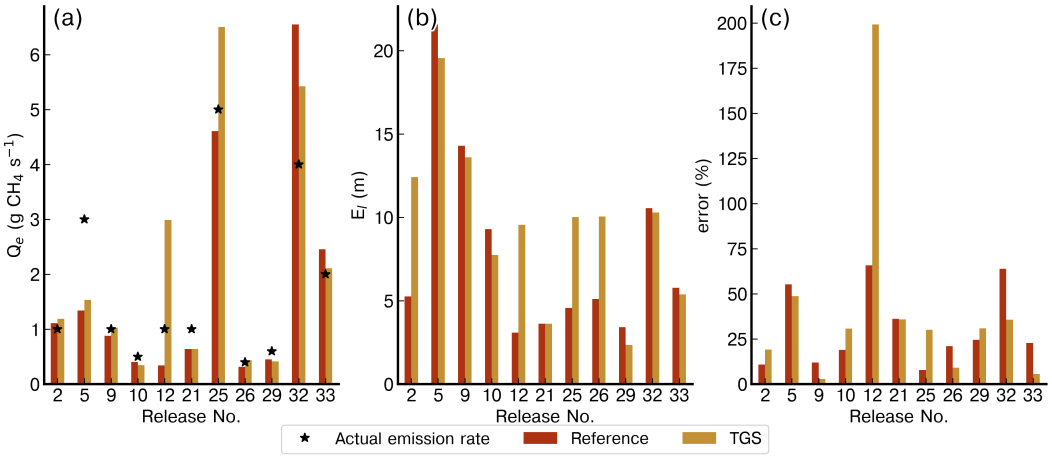

Figure A14. Comparison of the emission rate estimates (*Qe*), location error (*El*) and relative error on the rate estimates for the inversions assimilating the reference data and the reconstruction of the CH_4 from the TGS low-cost sensor based on the Polynomial model of ~~2nd~~ 2nd degree.

Table A1. Distribution of the releases by chamber. For each chamber is denoted with an 'o' the releases for which the TGS sensors produced valid measurements and with an 'x' the invalid ones.

Release number	Chamber A	C	D	E	F	H	Release number	Chamber A	C	D	E	F	H
1	-	-	-	x	x	o	19	o	o	-	o	o	o
2	o	-	-	o	o	o	20	o	o	-	o	o	o
3	-	-	-	o	o	o	21	o	o	-	o	o	o
4	-	-	-	o	o	o	22	-	o	-	o	o	-
5	o	-	o	o	o	-	23	-	-	-	o	-	o
6	o	-	o	o	o	-	24	o	o	x	-	o	o
7	o	-	o	o	o	-	25	o	o	o	o	o	o
8	o	-	o	o	o	-	26	o	o	x	o	-	o
9	o	o	o	o	o	-	27	o	o	-	-	-	x
10	o	o	x	x	o	-	28	o	o	-	-	-	o
11	o	x	-	-	-	-	29	o	o	-	-	o	o
12	x	x	o	o	o	-	30	o	o	-	-	-	o
13	-	x	o	o	o	o	31	-	o	-	-	-	-
14	o	o	o	o	o	o	32	o	o	-	o	-	o
15	o	o	-	-	o	-	33	x	o	-	o	-	o
16	o	-	-	x	-	-							
17	o	o	-	-	-	x							
18	o	o	-	-	o	o							

Table A2. Comparison of the emission rate ~~estimates~~ estimate (~~Q_s~~ *Qe*), location error (~~L_e~~ *El*) and ~~percentage of~~ relative error of ~~the~~ flux rate estimates ~~(Q_e)~~ for ~~the~~ inversions assimilating reference ~~instrument~~ gas analyser measurements and ~~the TGS low-cost sensor from~~ reconstructed ~~CH_4 of~~ TGS mole fractions using the ~~2nd~~ 2nd degree polynomial model.

Release N°	**N° Chambers**	**Controlled release emission rate ($g\ CH_4\ s^{-1}$)**	**Reference**			**TGS**		
			Q_e ($g\ CH_4\ s^{-1}$)	**E_l (m)**	**error (%)**	**Q_e ($g\ CH_4\ s^{-1}$)**	**E_l (m)**	**error (%)**
2	4	1.0	1.10	5.26	10.8	1.19	12,40	19,1
5	4	3.0	1.34	21.57	55.2	1.53	19,55	48,8
9	5	1.0	0.88	14.29	11.9	1.03	13,60	2,9
10	3	0.5	0.40	9.29	18.9	0.34	7,74	30,7
12	3	1.0	0.34	3.08	65.7	2.99	9,55	199,2
21	5	1.0	0.63	3.61	36.1	0.64	3,61	35,7
25	6	5.0	4.61	4.57	7.8	6.50	10,02	30,0
26	4	0.4	0.31	5.10	20.9	0.43	10,04	9,1
29	4	0.6	0.45	3.40	24.5	0.41	2,34	30,8
32	4	4.0	6.55	10.55	63.8	5.42	10,28	35,6
33	3	2.0	2.45	5.77	22.7	2.11	5,37	5,5
Average error				7.86	30.7		9.5	40.6
σ_{error}				5.46	20.3		4.6	51.9

Table A3. Summary of the tripods that were connected to each chamber.

Chamber	Tripod N°
A	1, 4, 6, 8, 9, 10, 11, 14, 15
C	2, 7, 9, 14, 15, 16
D	2, 3, 9, 10, 11, 12, 13, 16
E	1, 3, 4, 5, 10, 11, 12, 13, 16
F	2, 3, 4, 10, 11, 12, 13, 14, 15
H	4, 5, 6, 7, 12, 13, 14, 15

Table A4. Comparison between TGS sensors included on the low-cost logging systems during the TADI 2019 campaign.

Type	**Target gas**	**Approximate price**	**Comments**
2600	C_2H_5OH, C_4H_{10}, CO, H_2, CH_4	15 $us	Designed as a smoke detector.
2611-C00	CH_4, C_2H_5OH, C_4H_{10}, CO, H_2	20 $us	Designed for CH_4 detection. Fast response.
2611-E00	CH_4, H_2	20 $us	Designed for CH_4 detection. Increased selectivity due to a carbon filter installed on top of the sensing material.
2602	C_7H_8, H_2S, C_2H_5OH, NH_3, H_2	17 $us	High sensitive to VOC and odor gases.

Table A5. Summary of the species measured by each reference instrument.

Serial number / Code	Identifier	Species measured
CFKADS2286 / Picarro 1	Picarro CRDS G2401	CH_4, CO_2, CO
CFKADS2301 / Picarro 2	Picarro CRDS G2401	CH_4, CO_2, CO
CFKADS2194 / Picarro 3	Picarro CRDS G2401	CH_4, CO_2, CO
CFKADS2131 / Picarro 4	Picarro CRDS G2401	CH_4, CO_2, CO
CFIDS2067 / Picarro 5	Picarro CRDS G2201-i Isotopic	$^{13}CH_4$, $^{12}CH_4$, $^{13}CO_2$, $^{12}CO_2$
CFIDS2072 / Picarro 6	Picarro CRDS G2201-i Isotopic	$^{13}CH_4$, $^{12}CH_4$, $^{13}CO_2$, $^{12}CO_2$
LGR MGGA	Los Gatos Micro-portable Greenhouse gas analyzer	CH_4, CO_2

Table A6. Summary of the specifications of the chambers, the tripods to which each chamber was connected, the captured releases and the reference instrument collocated with each chamber.

Chamber	Figaro TGS sensors	Load resistor (Ω)	Other sensors	Chamber type	Tripod	# of measured releases	Reference instrument
A	2600 2611-C00 2611-E00	50K	DHT22 BMP280	Acrylic/glass	1, 4, 6 8, 9, 10 11, 14, 15	28	Picarro CFKADS2286
C	2600 2611-C00 2611-E00	50K	SHT75 BMP280	Acrylic/glass	2, 7, 9 14, 15, 16	24	Picarro CFIDS2072
D	2600 2611-C00 2611-E00	5K	SHT75 BMP280	Steel/glass	2, 3, 9 10, 11, 12 13, 16	14	Picarro CFKADS2301
E	2600* 2611-C00* 2611-E00*	5K	DHT22 SHT75 BMP180	Steel/glass	1, 3, 4 5, 10, 11 12, 13, 16	24	Picarro CFKADS2131
F	2600 2611-C00 2611-E00	50K	SHT75 BMP280	Acrylic/glass	2, 3, 4 10, 11, 12 13, 14, 15	25	Picarro CFKADS2194
H	2600 2611-C00 2611-E00	50K	SHT75 BMP180	Acrylic/glass	4, 5, 6 7, 12, 13 14, 15	22	LGR MGGA

* Two versions of each type.

Table A7. Computation time in seconds of the RSS matrix and the entire inversion including the preprocessing of the data for each release in the test set.

Release N°	N° Receptors	RSS matrix (s)	Data preprocessing + inversion (s)
2	4	0.148	1.497
5	4	0.099	1.498
9	5	0.092	1.260
10	3	0.034	0.992
12	3	0.073	1.428
21	5	0.094	1.286
25	6	0.146	1.511
26	4	0.156	1.859
29	4	0.152	1.923
32	4	0.094	1.425
33	3	0.086	1.455
Average		0.107	1.467